Global Biogeochemical Cycles

RESEARCH ARTICLE
10.1029/2022GB007386

Nitrogen Fixation in Mesoscale Eddies of the North Pacific Subtropical Gyre: Patterns and Mechanisms

Mathilde Dugenne[1,2,3], Mary R. Gradoville[4,5], Matthew J. Church[6], Samuel T. Wilson[1,2,7], Uri Sheyn[1,2,8], Matthew J. Harke[9,10], Karin M. Björkman[1,2], Nicholas J. Hawco[1], Annette M. Hynes[11], François Ribalet[11], David M. Karl[1,2], Edward F. DeLong[1,2], Sonya T. Dyhrman[9,12], E. Virginia Armbrust[11], Seth John[13], John M. Eppley[1,2], Katie Harding[4], Brittany Stewart[4,13], Ana M. Cabello[4,14], Kendra A. Turk-Kubo[4], Mathieu Caffin[1,2], Angelicque E. White[1,2], and Jonathan P. Zehr[4]

[1]Department of Oceanography, University of Hawai'i at Mānoa, Honolulu, HI, USA, [2]Daniel K. Inouye Center for Microbial Oceanography: Research and Education, University of Hawai'i at Mānoa, Honolulu, HI, USA, [3]Now at Sorbonne Université, CNRS, UM 7093, Laboratoire d'Océanographie de Villefranche-sur-Mer (LOV), Villefranche-sur-Mer, France, [4]Ocean Sciences Department, University of California Santa Cruz, Santa Cruz, CA, USA, [5]Now at Columbia River Inter-Tribal Fish Commission, Portland, OR, USA, [6]Flathead Lake Biological Station, University of MT, Polson, MT, USA, [7]Now at School of Natural and Environmental Sciences, Newcastle University, Newcastle upon Tyne, UK, [8]Now at Department of Biological Sciences, Virginia Tech, Blacksburg, VA, USA, [9]Lamont-Doherty Earth Observatory, Columbia University, Palisades, NY, USA, [10]Now at Gloucester Marine Genomics Institute, Gloucester, MA, USA, [11]School of Oceanography, University of Washington, Seattle, WA, USA, [12]Department of Earth and Environmental Sciences, Columbia University, New York, NY, USA, [13]Department of Earth Sciences, University of Southern California, Los Angeles, CA, USA, [14]Now at Centro Oceanográfico de Málaga, Instituto Español de Oceanografía, IEO-CSIC, 29640, Málaga, Spain

Abstract Mesoscale eddies have been shown to support elevated dinitrogen (N_2) fixation rates (NFRs) and abundances of N_2-fixing microorganisms (diazotrophs), but the mechanisms underlying these observations are not well understood. We sampled two pairs of mesoscale cyclones and anticyclones in the North Pacific Subtropical Gyre in 2017 and 2018 and compared our observations with seasonal patterns from the Hawaii Ocean Time-series (HOT) program. Consistent with previous reports, we found that NFRs were anomalously high for this region (up to 3.7-fold above previous monthly HOT observations) in the centers of both sampled anticyclones. In 2017, these elevated rates coincided with high concentrations of the diazotroph *Crocosphaera*. We then coupled our field-based observations, together with transcriptomic analyses of nutrient stress marker genes and ecological models, to evaluate the role of biological (via estimates of growth and grazing rates) and physical controls on populations of *Crocosphaera*, *Trichodesmium*, and diatom symbionts at the mesoscale. Our results suggest that increased *Crocosphaera* abundances in the 2017 anticyclone resulted from the alleviation of phosphate limitation, allowing cells to grow at rates exceeding grazing losses. In contrast, distributions of larger, buoyant taxa (*Trichodesmium* and diatom symbionts) appeared less affected by eddy-driven biological controls. Instead, they appeared driven by physical dynamics along frontal boundaries that separate cyclonic and anticyclonic eddies. No examined controls were able to explain our 2018 findings of higher NFRs in the anticyclone. A generalized explanation of elevated NFRs in mesoscale eddies remains challenging due to the interplay of eddy-driven bottom-up, top-down, and physical control mechanisms.

Mathilde Dugenne and Mary R. Gradoville contributed equally to this work.

Key Points:

- Nitrogen fixation rates in the centers of two anticyclonic eddies were anomalously high compared to historical Hawaii Ocean Time-series data
- High *Crocosphaera* abundance in one anticyclonic eddy was linked to both reduced phosphate limitation and reduced losses due to grazing
- Eddies affect specific diazotroph taxa through the physical accumulation of cells and through differential bottom-up and top-down forcing

Supporting Information:

Supporting Information may be found in the online version of this article.

Correspondence to:

M. Dugenne and M. R. Gradoville, mdugenne@hotmail.com; rgradoville@critfc.org

Citation:

Dugenne, M., Gradoville, M. R., Church, M. J., Wilson, S. T., Sheyn, U., Harke, M. J., et al. (2023). Nitrogen fixation in mesoscale eddies of the North Pacific Subtropical Gyre: Patterns and mechanisms. *Global Biogeochemical Cycles*, *37*, e2022GB007386. https://doi.org/10.1029/2022GB007386

Received 11 MAR 2022
Accepted 21 MAR 2023

1. Introduction

In the oligotrophic North Pacific Subtropical Gyre (NPSG), the supply of growth-limiting nutrients influences rates of photosynthesis in the sunlit surface ocean, determining the magnitude and variability of trophic transfer and the export of carbon (C) from the euphotic zone (Karl et al., 1996). Microorganisms with the ability to fix dinitrogen (N_2) into bioavailable ammonia, termed diazotrophs, introduce newly fixed nitrogen (N) to otherwise N-limited phytoplankton (Karl et al., 2002). N_2 fixation is especially important in warm, oligotrophic surface waters, where rates are generally limited by light, temperature, and concentrations of phosphate and/or iron (Letelier et al., 2019; Tang et al., 2019). At Station ALOHA (A Long-term Oligotrophic Habitat Assessment, 22.75°N, 158.00°W), the field site of the Hawaii Ocean Time-series (HOT) program, N_2 fixation fuels up to half of the new production and N export (Böttjer et al., 2017; Karl et al., 1997). Most N_2 fixation is controlled by unicellular diazotrophs (typically smaller than 10 μm), including the cyanobacteria UCYN-A (symbionts of haptophytes), UCYN-B (*Crocosphaera*), and UCYN-C (*Cyanothece*-like organisms) (Church et al., 2009; Zehr et al., 2001).

Other, larger cyanobacterial diazotrophs, including filamentous *Trichodesmium* and diatom-diazotroph associations (DDAs) with the symbiotic, heterocyst-forming *Richelia* and *Calothrix*, can also form episodic blooms and contribute appreciably to N_2 fixation. Finally, non-cyanobacterial diazotrophs are also present in the NPSG (Church, Jenkins, et al., 2005; Church, Short, et al., 2005; Farnelid et al., 2011), but the contribution of these organisms to N_2 fixation is uncertain (Moisander et al., 2017).

N_2 fixation rates (NFRs) at Station ALOHA are highly variable, ranging from ∼0.1 to 11 nmol N L^{-1} d^{-1} in near-surface waters (Böttjer et al., 2017, http://doi.org/10.5281/zenodo.6341629). Some of this variability is seasonal: NFRs generally peak during the late summer (Böttjer et al., 2017) when an annual pulse of particle export to the deep ocean has also been putatively linked to blooms of DDAs (Karl et al., 2012; Poff et al., 2021). However, several studies have also highlighted patchiness in both NFRs and diazotroph abundances over relatively small temporal (<2 days) and spatial (<30 km) scales (Gradoville et al., 2020; Robidart et al., 2014), suggesting that submesoscale and mesoscale processes may influence diazotroph distributions in the NPSG. Such physical disturbances of the upper pelagic zone are regular features of this habitat (Rii et al., 2021); for example, over a 23-year period of near-monthly sampling by the HOT program at Station ALOHA, 31% of the sampling occasions coincided with the presence of a trackable mesoscale eddy (Barone et al., 2019).

Through uplift or depression of the pycnocline, eddies perturb microbial populations by altering nutrient and light fields (Benitez-Nelson et al., 2007; McGillicuddy & Robinson, 1997). As a result, mesoscale eddies, especially cyclonic eddies that drive upward displacement of isopycnal surfaces (together with associated nutrients) across the upper ocean light gradient, have been linked to elevated phytoplankton biomass and high rates of primary production in the open ocean (McGillicuddy & Robinson, 1997). There is growing evidence that diazotrophic community structures and NFRs are also modified by mesoscale eddies. High NFRs have been observed in anticyclonic eddies in many ocean regions, including the South Pacific Ocean, Indian Ocean, South China Sea, and Mediterranean Sea (Holl et al., 2007; Liu et al., 2020; Löscher et al., 2016; Rahav et al., 2013). At Station ALOHA, the highest NFRs have been observed under conditions of elevated sea surface height (characteristic of anticyclonic eddies) in summer months (Böttjer et al., 2017; Church et al., 2009). Elevated abundances of *Trichodesmium*, DDAs, and *Crocosphaera* have been reported to be associated with anticyclonic eddies in both the North Atlantic and North Pacific Oceans (Cheung et al., 2020; Davis & McGillicuddy, 2006; Fong et al., 2008; Olson et al., 2015; Taboada et al., 2010; Wilson et al., 2017).

These studies have highlighted multiple processes that could influence N_2 fixation in eddies of different polarities. For example, elevated NFRs and *Crocosphaera* abundances were linked to severe N-depletion in the surface waters of anticyclones, presumably driven by the depression of isopycnal surfaces (Liu et al., 2020; Wilson et al., 2017). In addition, although poorly characterized, high rates of grazing on diazotrophs and their hosts have been reported within mesoscale eddies of both polarities (Dugenne et al., 2020; Landry et al., 2008; Wilson et al., 2017). Finally, the physical movement of water, both vertically and horizontally, due to mesoscale circulation, can lead to the physical accumulation of buoyant diazotrophs (e.g., *Trichodesmium*) (Guidi et al., 2012; Olson et al., 2015). All of these mechanisms are modulated by specific life history traits (e.g., buoyancy, size, symbiosis) and potential adaptations of individual taxa, suggesting that understanding diazotrophic diversity and activity within eddies is a prerequisite to identifying the mechanisms driving variability in bulk NFRs. Effectively, mesoscale and sub-mesoscale features can impact both bottom-up and top-down processes controlling diazotroph diversity and activity. The relative influence of these controls is important in determining diazotroph abundance as well as the magnitude of new N delivered to the system.

In this study, we examined cyanobacterial diazotroph abundances and NFRs associated with two pairs of mesoscale eddies (cyclones and anticyclones) sampled in the NPSG and compared these data to patterns from the HOT program for regional and seasonal contexts. We used these observations, together with environmental data, metatranscriptomes, and ecological models, to evaluate the importance of bottom-up, top-down, and physical control mechanisms in driving the mesoscale distribution and activity of diazotroph populations.

2. Material and Methods

2.1. Characterization and Sampling of Eddy Pairs

In 2017 and 2018, two field expeditions sampled mesoscale eddies in the region north of the Hawaiian Islands. Observations took place 26 June–15 July 2017 during the Microbial Ecology of the Surface Ocean-Simons

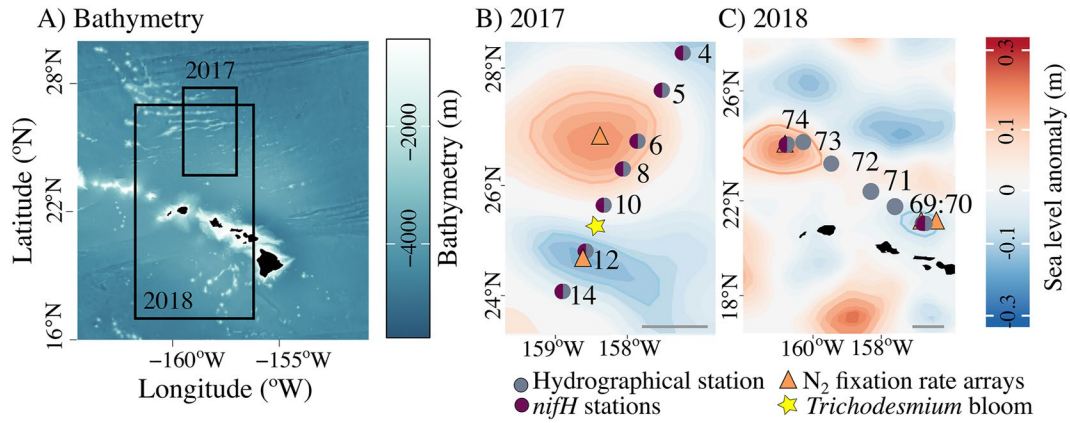

Figure 1. Bathymetry of the study area encapsulating the cruise regions in 2017 and 2018 (a). Contours of sea-level anomalies from 07 July 2017 (b) and 06 April 2018 (c), downloaded from the Copernicus Marine and Environment Monitoring Service (http://www.marine.copernicus.eu) and corrected according to Barone et al. (2019), showing the sampling locations for *nifH* gene abundances (purple circles), hydrographical stations (blue circles), a *Trichodesmium* bloom (yellow star), and N_2 fixation rates (triangles) across each pair of eddies. Note that surface diazotroph cell abundances were continuously measured by autonomous flow cytometry during each cruise. Sampled cyclones are indicated by negative sea-level anomalies (−0.1 m blue contour) and anticyclones by positive sea-level anomalies (0.1 m red contour). Note that the 2017 anticyclone moved westward between the time we targeted the eddy center for transect (including *nifH* collection) and the Lagrangian sampling (including NFR measurement) (∼1 week apart). Scale bars: 100 km.

Collaboration on Ocean Processes and Ecology cruise (MESO-SCOPE, KM1709, *R/V Kilo Moana*) and 27 March–10 April 2018 during the Hawaiian Eddy Experiment (FK180310, *R/V Falkor*). Prior to each cruise, cyclonic and anticyclonic eddies were identified via satellite-derived sea-level anomalies (SLA) distributed by the Copernicus Marine Service (marine.copernicus.eu/). Daily SLA maps (Figure 1) were corrected for the multi-year trend and seasonal cycle following Barone et al. (2019). Eddies were tracked back in time to determine the stage, age, and average SLA during the sampling period (Text S1 and Table S1 in Supporting Information S1).

Both cruises included an eddy mapping phase, where sampling occurred along a transect spanning one eddy to the other in order to characterize the water column, quantify diazotrophs via *nifH* gene abundances and automated imaging flow cytometry cell counts, and measure NFRs. They also included time-resolved Lagrangian surveys that sampled along the drift trajectories of Surface Velocity Program (Pacific Gyre) drifters in one or both eddy centers (drogue centered at 15 m), with continuous imaging of near surface plankton communities to assess high resolution temporal dynamics. During the continuous sampling in eddy centers, we observed little variation in temperature and salinity in the near surface layer, with standard deviations ranging between 0.08–0.22ºC and 0.005–0.03, respectively, indicating that we likely tracked the same water mass throughout each survey (data not shown).

Photosynthetically active radiation (PAR) at the sea surface was measured using a shipboard cosine collector LI-190 (LI-COR Environmental, Lincoln, NE, USA). Downwelling PAR was measured at 1 m intervals using a free-falling optical profiler (Satlantic HyperPro, Sea-Bird Scientific, Bellevue, WA, USA) and corrected by a factor of 1.2 to convert downwelling irradiance into scalar irradiance (Letelier et al., 2017; Wozniak et al., 2003). Both sea surface and downwelling PAR measurements were used to compute the fraction of incident PAR (%) at discrete depths.

A Conductivity, Temperature, and Depth (CTD, Sea-Bird Scientific) sensor attached to a rosette sampler was used to measure depth profiles of temperature, salinity, and derived potential density. Mixed layer depth (MLD) was calculated using a 0.03 potential density offset relative to 10 m (de Boyer Montégut et al., 2004). Seawater samples collected from discrete depths using 24 × 10 L Niskin® bottles mounted to the rosette frame were used to measure soluble reactive phosphorus (hereafter phosphate, PO_4^{3-}) concentrations (precision of ±1 nmol L^{-1} and detection limit of 3 nmol L^{-1}) (Karl & Tien, 1992) and nitrate + nitrite ($NO_3^- + NO_2^-$) concentrations (detection limit of 1 nmol L^{-1}) (Foreman et al., 2016). Profiles of PO_4^{3-}, $NO_3^- + NO_2^-$, and $[NO_3^- + NO_2^-]$: $[PO_4^{3-}]$ ratios are shown in Figure S1 in Supporting Information S1, along with same-month measurements from Station ALOHA.

Dissolved Fe (dFe) for the 2017 cruise was collected using a trace metal clean sampling rosette with external spring bottles (Ocean Test Equipment). For the 2018 cruise, samples for dFe were collected in Go-Flo® bottles mounted on a non-metallic line and triggered with a PTFE messenger. Dissolved iron concentrations were determined by inductively coupled plasma mass spectrometry (ICP-MS) using isotope dilution (Hawco et al., 2021; Pinedo-González et al., 2020). The accuracy of these measurements was confirmed by analyzing reference seawater samples, GS (0.55 ± 0.01 nM Fe, $n = 3$) and GSP (0.19 ± 0.03 nM Fe, $n = 3$), provided by the GEOTRACES community (www.geotraces.org/standards-and-reference-materials).

2.2. N_2 Fixation Rates

NFRs were measured on all cruises using a modification of the $^{15}N_2$ uptake method of Montoya et al. (1996), in which the $^{15}N_2$ tracer was added as $^{15}N_2$-enriched seawater to avoid incomplete dissolution of $^{15}N_2$ gas (Mohr et al., 2010; Wilson et al., 2012). Prior to each cruise, surface seawater was collected from Station ALOHA, filtered through a 0.2 μm in-line filter (AcroPak 1000 capsule, Pall Corporation, Port Washington, NY, USA) and transported in the dark to the laboratory. There, the seawater was degassed, injected with ∼13 mL $^{15}N_2$ gas (99 atom %, Cambridge Scientific, Watertown, MA, USA) per L seawater, and manually agitated to dissolve the gas bubble, as described by Wilson et al. (2012). The resulting $^{15}N_2$-enriched seawater was dispensed into crimp-sealed, glass serum bottles, stored at 4°C for less than 1 week, and brought to sea. To initiate incubations, 100 mL of seawater was withdrawn from each full 4.4 L incubation bottle and replaced with 100 mL of $^{15}N_2$-enriched seawater. The $^{15}N/^{14}N$ ratio of each batch of $^{15}N_2$-enriched seawater was measured using membrane inlet mass spectrometry according to Ferrón et al. (2016). These values were used to calculate the initial atom % of $^{15}N_2$ for each incubation. A recent study by White et al. (2020) indicates that measuring the $^{15}N_2$ atom % of the enriched seawater rather than the final inoculum may lead to inaccurate initial $^{15}N_2$ atom % values, which for the enriched seawater preparation method used for the eddy and HOT observations reported in this study, could have led to a <20% underestimation of final calculated rates.

NFRs were measured using free-drifting in situ arrays deployed at eddy centers (Figure 1). Seawater was collected pre-dawn from 5, 25, 45, 75, 100, and 125 m depths using the CTD rosette Niskin® sampling bottles. Seawater was subsampled into triplicate 4.4 L acid-washed, seawater-rinsed polycarbonate bottles, which were spiked with $^{15}N_2$ tracer (see above), attached to the free-floating arrays, and incubated for 24 hr at the depth from which they had been collected. Incubations were terminated by filtering (via a peristaltic pump or vacuum filtration) through pre-combusted (5 hr at 450°C) 25 mm glass fiber filters (GF/F, Whatman, Maidstone, UK). Additional 4.4 L seawater samples were collected from each sampling depth for $\delta^{15}N$ natural abundance measurements; these samples were immediately filtered at the start of each incubation. All filters were frozen at −20°C or −80°C and transported to the laboratory, where they were dried at 60°C overnight and pelleted into tin capsules (Costech Analytical Tech Inc, Valencia, CA, USA). Concentrations and isotopic composition ($\delta^{15}N$) of particulate N were analyzed via continuous-flow isotope ratio mass spectrometry using a Carlo-Erba EA NC2500 coupled with Thermo Finnigan DeltaPlus XP at the University of Hawai'i Biogeochemical Stable Isotope Facility. NFRs and detection limits were calculated according to Montoya et al. (1996) (Table S2 in Supporting Information S2).

Time-series NFRs measured at Station ALOHA are also presented to provide context for the two eddy cruises. A subset of the time-series (2012–2014) has previously been published by Böttjer et al. (2017); for this study, we extend that time series through 2019. These extended time-series measurements followed procedures identical to those described in Böttjer et al. (2017).

2.3. Diazotroph Abundances

2.3.1. DNA Extraction and *nifH* Gene Quantification

The *nifH* genes of seven major cyanobacterial diazotroph groups were quantified using digital droplet polymerase chain reaction (ddPCR). During the 2018 cruise, seawater for subsequent ddPCR analyses was collected from depth profiles at the same locations sampled for $^{15}N_2$ incubations. During the 2017 cruise, seawater for ddPCR was collected from depth profiles within each eddy but from separate locations than those used for the $^{15}N_2$ arrays (Figure 1). For both cruises, seawater samples were collected from a rosette sampler and subsampled into duplicate (2018) or single (2017) 4.4 L acid-washed, milliQ-rinsed polycarbonate bottles. A peristaltic pump was used to filter 4 L of seawater through 0.2 μm pore-size Supor® membranes (Pall), which were placed into

microcentrifuge tubes containing mixtures of 0.1- and 0.5-mm glass beads (Biospec Products, Bartlesville, OK, USA), flash-frozen in liquid N_2, and stored at −80°C until analysis.

DNA was extracted from filters with a QIAcube instrument (Qiagen, Venlo, Netherlands) using the DNeasy Plant Mini Kit. Extractions followed the manufacturer's protocol with additional steps of three flash freeze/thaw cycles, bead-beating for 2 min, and a Proteinase K treatment, as described by Moisander et al. (2008). The final DNA elution volume was 100 µL. DNA extracts were stored at −20°C prior to ddPCR. Duplicate ddPCR reactions were performed for each sample using primers and probes, which targeted the following groups: *Trichodesmium* (Church, Jenkins, et al., 2005), UCYN-A (targeting the small UCYN-A1 sublineage, Church, Jenkins et al., 2005), *Crocosphaera* (UCYN-B, Moisander et al., 2010), *Cyanothece*-like organisms, (UCYN-C, Foster et al., 2007), *Richelia* associated with *Rhizosolenia* (Het-1, Church, Short, et al., 2005), *Richelia* associated with *Hemiaulus* (Het-2, Foster et al., 2007), and *Calothrix* associated with *Chaetoceros* (Het-3, Foster et al., 2007). Descriptions of ddPCR reaction setup, droplet generation, thermocycling, thresholding, and detection limit calculations are provided in Gradoville et al. (2021).

For the temporal context, we also report *nifH* gene abundances of UCYN-A, UCYN-B, *Trichodesmium*, Het-1, Het-2, and Het-3, measured at Station ALOHA between 2004 and 2017 (data set https://doi.org/10.5281/zenodo.4477269). For these measurements, *nifH* gene abundances were determined using quantitative PCR (qPCR); details on sample collection, DNA extraction, and qPCR are provided in Church et al. (2009). All qPCR assays except for Het-2 and Het-3 used the same primer/probe sets as the corresponding ddPCR assays for the eddy cruises. Het-2 was quantified using the primer/probe sets of Church et al. (2008), while Het-3 used the same forward and reverse primers used for ddPCR, but the probe sequence contained an extra adenine on the 3' end.

2.3.2. Diazotroph Cell and Filament Enumeration by Autonomous Flow Cytometry

Concentrations of large (>4 µm in diameter or length, imposed by the size detection limit of the instrument) free-living and filamentous diazotrophs, including *Trichodesmium* (single filaments), *Richelia* (free and symbiotic heterocyst-containing filaments), *Calothrix* (unattached and epiphytic heterocyst-containing filaments), and large-size *Crocosphaera*-like organisms (free-living, hereafter referred as *Crocosphaera*), were estimated by automated imaging flow cytometry equipped with a 635 nm red laser (Imaging FlowCytobot [IFCb], McLane, East Falmouth, MA, USA) during the 2017 and 2018 cruises. Approximately 5 mL samples were collected every ∼20 min from the ship's uncontaminated underway system (∼7 m depth). Discrete bucket samples from a visual *Trichodesmium* bloom were also analyzed on the IFCb in 2017 (Figure 1). During the analysis, individual images of single or colonial cells were collected along with their optical fingerprints: light scattering and red fluorescence (680 ± 30 nm) emitted by chlorophyll and phycocyanin pigments. The latter is found in N_2-fixing cyanobacteria (Boatman et al., 2018; Webb et al., 2009; Zeev et al., 2008), and, along with additional morphological traits (e.g., size, filaments), can help discriminate diazotrophs from other phytoplankton. A training set of images was used to classify organisms to the genera level based on morphological traits, as described in Dugenne et al. (2020). The output of the random forest classifier (Sosik & Olson, 2007) was corrected by manually annotating misclassified images to provide accurate estimates of cell and filament concentrations of individual genera. To compare the cell counts of rare, filamentous diazotrophs with *nifH* gene abundances, we binned consecutive samples in 2 hr intervals (in order to integrate a larger volume and lower the detection limit) and manually estimated the number of cells per filament.

Small-size *Crocosphaera* (2–4 µm) were enumerated using an autonomous SeaFlow flow cytometer (Ribalet et al., 2019). Briefly, the SeaFlow was used to continuously sample surface seawater from the ship's uncontaminated underway system, acquiring optical measurements of light scatter, red fluorescence, and orange fluorescence (characteristic of the phycoerythrin-containing *Crocosphaera*) at 3 min intervals. The population of small-size *Crocosphaera* was gated over time to estimate abundances during time points close (less than 2 hr) to collection times of the discrete *nifH* gene abundance samples.

2.4. Metatranscriptomic Analysis of Stress Marker Genes

For insight into possible diazotroph growth limitation by P and Fe in eddy centers, we examined transcriptional patterns in P- and Fe-stress marker genes from samples collected during the 2017 cruise. Metatranscriptome samples were collected within the mixed layer (15 m) and the deep chlorophyll maximum (DCM, located at depths of 106 ± 5 m and 123 ± 5 m in the cyclone and anticyclone, respectively) at ∼4 hr intervals for three days

during the Lagrangian sampling of the cyclonic and anticyclonic eddies ($n = 18$ for each eddy). Seawater samples were collected using the rosette sampler and seawater (1 L) was filtered through 25 mm diameter, 0.2 µm Supor® membranes (Pall) housed in Swinnex™ units (Millipore Sigma) using a peristaltic pump. Filtration times were limited to 15–20 min. Immediately following filtration, filters were placed in RNALater (Invitrogen, Waltham, MA, USA) and stored at –80°C until they were processed.

Sample and data processing were performed using the methods described by Gifford et al. (2016) and Wilson et al. (2017). Briefly, sample processing steps included RNA extraction, spiking with internal controls, cDNA synthesis, and sequencing using Illumina NextSeq 500 v2. Approximately two million 150-bp paired-end reads were produced for each sample; raw sequences are available on NCBI SRA under project number PRJNA596510. Reads were screened for quality, trimmed, and assembled after removing sequencing primers. Genes were mapped to the ALOHA 2.0 gene catalog (Luo et al., 2020), and annotated using the Genome Taxonomy Database (GTDB, Parks et al., 2018). Raw sequence reads are available on NCBI SRA under project number PRJNA596510. Transcript counts were normalized to internal standards to account for methodological biases among samples, including library preparation and sequencing, and also normalized to the volume of water filtered for each sample as previously described (Wilson et al., 2017). Values above detection limits were further normalized to the total sample expression sum within each genus-level annotation. This step was required in order to compare eddy differential gene expression based on cellular regulation rather than the total number of cells. Transcripts of P- and Fe-stress marker genes (genes with higher expression levels under low P and Fe concentrations, as reviewed by Stenegren (2020) and Snow et al. (2015)) were extracted from the data set according to functional annotations assigned by comparison to the Kyoto Encyclopedia of Genes and Genomes (P-stress genes: *ppK*, *sqdB*, *pstS*, *sphX*, *phoD*, and *phnE*; Fe-stress genes: *feoB*, *idiA*, and *isiA*).

Several genes exhibited diel expression patterns. To account for the expression periodicity and evaluate the differences in gene transcript abundances between eddies, we normalized the abundance of transcripts above detection limits within each eddy to the overall average of each gene transcript from both eddies over the entire time-series (generating a single value per gene/taxa computed from all the time points, with the exception of time points under detection limits). This step facilitated comparisons of different gene transcripts having large variations in their diel baseline and maximum transcript expression levels.

The statistical significance of the relative change in expression was tested using the Kruskal-Wallis test (R function "kruskal.test"). All gene transcripts from UCYN-A and *Calothrix*, as well as the transcripts of several genes from *Richelia* and *Trichodesmium*, were excluded from analyses as their abundances always fell below the detection limit in at least one eddy, especially in samples collected at the DCM.

2.5. Diazotroph Population Models

2.5.1. Bottom-Up Control on Diazotroph Populations

We used an ecophysiological model (Follett et al., 2018; McGillicuddy, 2014; Stukel et al., 2014) to evaluate how measured abiotic factors (nutrient concentrations, light, and temperature) may have influenced diazotroph intrinsic growth rates (μ; per day) across the pairs of eddies. Predictions are based on the ecophysiological parameters of cyanobacterial diazotroph taxa derived from laboratory cultures and modeling studies examining the effect of temperature (T), average instantaneous scalar PAR (E), PO_4^{3-}, and dFe concentrations on growth rates (Table S3 in Supporting Information S1). Model assumptions and caveats, including but not limited to error propagation and parameter uncertainty, are described in Text S2 in Supporting Information S1.

We integrated the effects of abiotic factors on population growth rates by scaling the temperature- and light-dependent theoretical maximum growth rate of each taxon ($\mu_{max} \times f_\mu(T) \times f_\mu(E)$) to the relative change in growth rate predicted by the main limiting nutrient ($\min(f_\mu(PO_4^{3-}), f_\mu(dFe))$), according to Liebig's law of the minimum:

$$\mu\left(T, E, PO_4^{3-}, dFe\right) = \mu_{max} \times f_\mu(T) \times f_\mu(E) \times \min\left(f_\mu\left(PO_4^{3-}\right), f_\mu(dFe)\right) \quad (1)$$

where f_μ designate unitless limiting functions (Equations 2, 3, and 5) representing the changes in diazotroph growth rates relative to their maximum. We determined the dominant limiting factors amongst all abiotic factors (including light and temperature) by identifying the variable yielding the minimum relative growth rates computed from Equations 2, 3, and 5.

The change in relative growth rate as a function of T followed Equation 2:

$$f_\mu(T) = Q_{10}^{\frac{T-T_{\text{opt}}}{10}} \tag{2}$$

with T_{opt} (°C) the optimal temperature for which $f_\mu(T_{\text{opt}}) = 1$ and Q_{10}, the Arrhenius coefficient corresponding to the change of growth rate over a 10°C temperature increase (reported in Table S3 in Supporting Information S1 for individual diazotroph taxa). Note that $f_\mu(T)$ can be >1 for temperatures above the thermal optimum of diazotrophs; however, this condition did not occur in 2017 or 2018.

The change in relative growth rate as a function of E (μmol quanta m^{-2} s^{-1}) was predicted using a modification of the hyperbolic tangent function described in Jassby and Platt (1976):

$$f_\mu(E) = \tanh\left(\frac{\alpha(E - E_c)}{\mu_{\max}}\right) \tag{3}$$

with E_c (μmol quanta m^{-2} s^{-1}), the compensation light intensity. The light saturation parameter, E_k (μmol quanta m^{-2} s^{-1}), is then derived using the maximum growth rate, $\mu_{\max}$, reported in Table S3 in Supporting Information S1 and the initial slope of μ-E curve presented in the literature, α, as

$$E_k = \frac{\mu_{\max}}{\alpha} + E_c \tag{4}$$

with $f_\mu(E)$ tending to 1 for $E > E_k$.

Finally, Michaelis-Menten kinetics was used to express the change in relative growth rate as a function of PO_4^{3-} and dFe concentration (nmol L^{-1}):

$$f_\mu\left(PO_4^{3-}\right) = \frac{\left(PO_4^{3-} - PO_4^{3-}{}_{\min}\right)}{\left(PO_4^{3-} - PO_4^{3-}{}_{\min}\right) + k_{PO_4^{3-}}}, f_\mu(d\text{Fe}) = \frac{(\text{dFe} - \text{dFe}_{\min})}{(\text{dFe} - \text{dFe}_{\min}) + k_{\text{Fe}}} \tag{5}$$

with $\text{dFe}/PO_4^{3-}{}_{\min}$, the minimum concentration required by diazotrophs to grow, and $k_{PO_4^{3-}/\text{Fe}}$, the half-saturation coefficient, corresponding to the corrected nutrient concentration (nmol L^{-1}) at which f_μ equals 0.5.

All models were fitted to published culture data (references in Table S3 in Supporting Information S1) using the nonlinear least-squares R function "nls" and parameter uncertainties, determined by bootstrap using the R function "nlsBoot", were propagated using "predictNLS" from the R package propagate. We tested the differences in intrinsic growth rate estimates between eddies of opposite polarity using generalized linear regression, assuming a quasi-binomial distribution (which is typically assumed for biological rates (Crawley, 2013) and agreed with the independent predictions of *Crocosphaera* in situ growth rates derived from the detection of dividing cells in 2017 (Dugenne et al., 2020)), weighted by the uncertainties of the estimates with the R function glm($\mu \sim$ Eddy, family = quasibinomial(link = "logit"),weights = $1/\sigma^2(\mu(\text{T,E, } PO_4^{3-}\text{,dFe}))$), where the explanatory variable "Eddy" corresponds to eddy polarity. We used the R function "anova" to perform a Chi-square test between this model and the null model, in which growth rates are considered constant across eddies, glm($\mu \sim 1$,family = quasibinomial(link = "logit"),weights = $1/\sigma^2(\mu(\text{T,E, } PO_4^{3-}\text{,dFe}))$). We acknowledge that the uncertainty of many of the parameters are not known for cultured strains, let alone for mixed assemblages, with unknown strain compositions in situ, which is an important caveat of many forms of models (see discussion in Schartau et al. (2017) for a thorough discussion of this topic).

2.5.2. Predation Control on Diazotroph Populations

We explored how mesoscale eddies affected estimates of diazotroph grazing rates using a standard statistical predator-prey model. The predation model relied on co-occurrence interactions between a given diazotroph (i.e., *Crocosphaera*, *Richelia*, *Calothrix*, *Trichodesmium*) and potential predators, based on abundance data from the IFCb (see Dugenne et al., 2020 for a description of the predator-prey model and Section 2.3.2 above for a brief description of the IFCb). More specifically, we leveraged the IFCb images to (a) determine significant interactions within a generalized predator-prey model (Equation 6) and (b) visualize ingested diazotrophic prey. We relied on the temporal dynamics of diazotrophic prey (x_i, cells or filaments L^{-1}) and putative predators (x_j, cells L^{-1}),

measured in the eddy centers throughout the Lagrangian surveys (hence, assuming that population dynamics are only driven by growth and loss rates) to identify significant interactions (a_{ij}):

$$\frac{dx_i}{dt} = x_i\left(r_i + \sum_j a_{ij}x_j\right) \tag{6}$$

The term r comprised a linear intrinsic growth rate and a linear loss rate due to processes not explicitly accounted for with the biological interactions tested (e.g., viral lysis, programmed cell death, additional grazers not imaged by the IFCb, vertical migration, mixed layer entrainment, and/or sinking). A similar model has previously been used to assess the short-term variability of grazing rate estimates (Dugenne et al., 2020); however, here we simplified this model to have fixed parameters in each eddy center (e.g., throughout each Lagrangian survey) in order to compare grazing rates between eddies.

In the current model, the strength of the interaction between populations i and j is determined by the coefficient a_{ij} and by population abundances; a_{ij} can be interpreted as different biological rates depending on the type of interaction. When coefficients a_{ij} and a_{ij} are negative and positive, respectively, j grows at i's expense, as would a putative grazer of the diazotroph i. All pairs of interaction coefficients were estimated using a multi-linear regression model fitted to the changes in population abundances throughout the Lagrangian sampling period within individual eddies as follows:

$$\frac{\Delta ln(x_i)}{\Delta t} = y = r_i + \sum_j a_{ij}x_j \tag{7}$$

with Δt, a 1 hr interval based on the sensitivity analysis presented in Text S3 in Supporting Information S1, yielding an average uncertainty (calculated as the ratio of the standard error over the estimate for the regression coefficient) of 12 ± 6% of $a_{ij,}$ the linear coefficient for the interaction with population j (Figure S2a in Supporting Information S1), corresponding to the number of prey consumed per predator per time interval (see Supporting Information S2 in Dugenne et al. (2020) for a detailed description of model parameters units and definitions), and $r_{i,}$ the intercept of the linear regression per unit of time interval. Since the regression included a large number of coefficients, accommodating 103 populations in 2017 and 89 populations in 2018, we used a regularized Lasso regression implemented in the "glmnet" R package to penalize non-significant interactions (Tibshirani et al., 2012). This approach allowed us to fit the multi-linear regression only based on significant coefficients (instead of performing a standard multi-linear regression and re-fitting the same observations after excluding non-significant interactions to retrieve *post-hoc* coefficients). *P*-values of individual grazing rate estimates are shown in Figure S2b in Supporting Information S1 and a time-series of diazotrophs and their putative grazers, as well as model fit 95% confidence intervals and R^2 values, is presented in Figure S3 in Supporting Information S1.

We also looked for visual evidence of diazotrophic prey ingestion using the IFCb images from 2017 to 2018 to confirm the significant interaction between diazotrophs and their putative grazers. Significant coefficients were sorted to determine the importance of individual protist consumption on specific diazotrophic prey based on g_j (d^{-1}), the product of coefficient a_{ij} and the abundance of grazer population j. The overall rates of grazing on a diazotroph taxon, g (d^{-1}), was calculated as the sum of all the individual grazing rates:

$$g = \sum_j g_j = \sum_j a_{ij}x_j \tag{8}$$

with a_{ij} negative and a_{ji} positive. Grazing rate estimates, corresponding to the rate of diazotrophic prey consumption by putative grazers in specific eddies, are expressed in units per day, and further compared to diazotroph intrinsic growth rate estimates calculated from Equation 1 to estimate their grazing pressure (the ratio of predicted grazing rate to growth rate, equivalent to the proportion of newly produced diazotroph cells lost by grazing). The uncertainty of g was estimated by propagating errors from a_{ij} and x_j. We note that this approach to model grazing rates makes a number of assumptions, including but not limited to (a) truly Lagrangian sampling, (b) fixed biological rates through Lagrangian sampling, (c) that the visualization of ingested prey is conclusive evidence of grazing, (d) that population changes were neither due to microscale patchiness of either predator or prey driven by submesoscale or other forcings nor by significant displacement of motile grazers, and (e) that interactions of those identified predators with ingested prey represent grazing rather than another biological

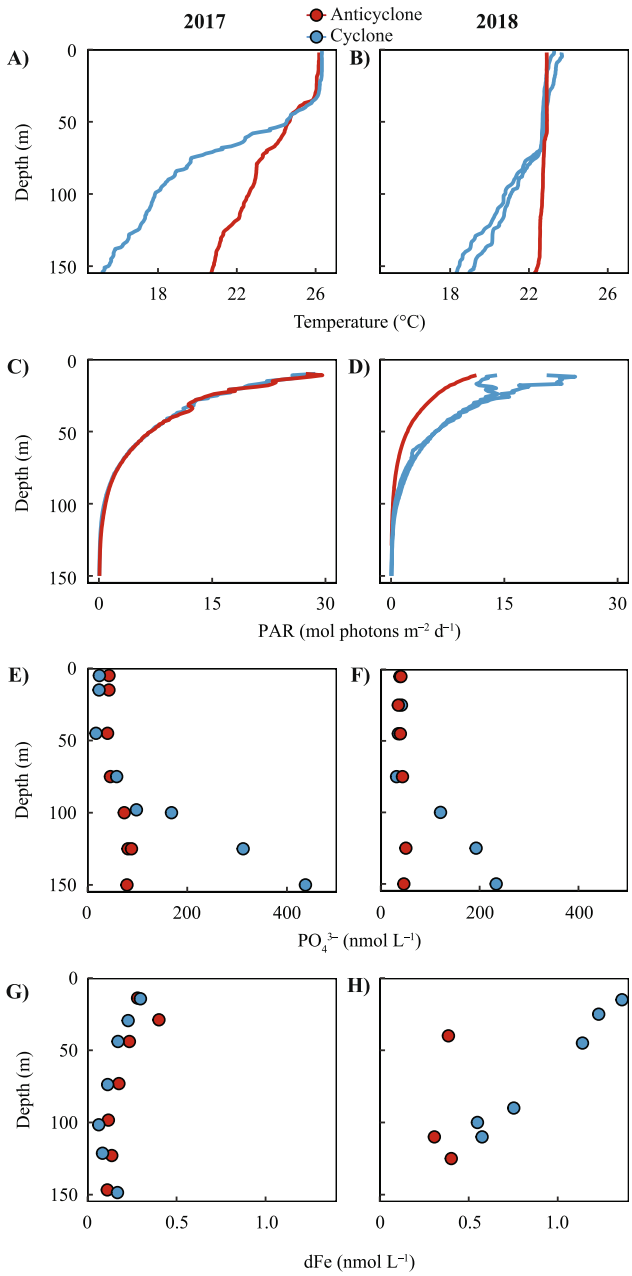

Figure 2. Depth profiles of temperature (a, b), Photosynthetically active radiation (PAR) (c, d), PO_4^{3-} concentrations (e, f), and dFe concentrations (g, h) on the 2017 (left) and 2018 (right) cruises. Red and blue indicate observations from the anticyclonic and cyclonic eddies, respectively. Profiles of temperature and PAR are from the days and locations of the N_2 fixation measurements (note that N_2 fixation rates were measured twice within the 2018 cyclone); PO_4^{3-} and dFe concentrations were measured at nearby stations within the same eddy.

association (e.g., symbiosis, which was also tested in our multilinear model; see interactions and correlation matrices available at https://doi.org/10.5281/zenodo.7540299).

3. Results

3.1. Mesoscale Patterns in Environmental Conditions, NFRs, and Diazotroph Abundances

3.1.1. Physical and Biogeochemical Setting

Sampled eddies varied by age and phase as well as by in situ light, temperature, and nutrient concentrations. At the time of sampling, both anticyclones were in a stable phase (defined by the fluctuations of SLA amplitude in the eddy centers, Table S1 in Supporting Information S1) and both cyclones were in a weakening phase. The two pairs of eddies were sampled in different seasons: summer (July) in 2017 and early spring (March–April) in 2018. Physical variables generally followed expected seasonal trends, with higher sea surface temperature and daily incident light in the 2017 cruise (Figure 2) and the deepest mixed layer observed in the 2018 cruise (2018 anticyclone MLD = 50.3 ± 17.8 m; mean MLD in other eddies ranged 17.8–30.6 m, Table S1 in Supporting Information S1). Temperature and in situ light flux decreased with depth, except in the 2018 anticyclone, where temperature was nearly constant within the upper 150 m (Figure 2). Near-surface temperatures were similar between eddies within each cruise; however, temperatures were lower in the lower euphotic zone of the cyclonic eddies (Figure 2), consistent with the uplift of deeper isopycnals. Daily integrated light did not vary between eddies during the 2017 cruise, while in the 2018 cruise, lower daily integrated light was observed in the anticyclone due to cloud cover on the day of sampling (Figure 2).

PO_4^{3-} concentrations varied with depth and eddy polarity. PO_4^{3-} concentrations were lowest at the surface and increased with depth, except for the 2018 anticyclone, in which concentrations were relatively stable within the upper 150 m, consistent with the near-homogenous temperature profile (Figure 2) and deep downwelling intensified by winter mixing (Table S1 in Supporting Information S1). At depths of 100–150 m, PO_4^{3-} concentrations were always higher in cyclones than in anticyclones (Figure 2) due to eddy-induced changes in the depths of isopycnal surfaces. In contrast, during the 2017 cruise, PO_4^{3-} concentrations in the upper 45 m were greater in the anticyclone (42 ± 2 nmol L^{-1}) than in the cyclone (21 ± 4 nmol L^{-1}) (Figure 2). During the 2018 cruise, PO_4^{3-} concentrations (range: 35–42 nmol L^{-1}) and inorganic $[NO_3^- + NO_2^-]$: $[PO_4^{3-}]$ ratios (0.15–0.34 mol:mol) in the upper 45 m did not differ between the cyclonic and anticyclonic eddies (Figure 2). $NO_3^- + NO_2^-$ generally followed the same pattern as PO_4^{3-} concentrations on both cruises (Figure S1 in Supporting Information S1). All surface molar $[NO_3^- + NO_2^-]$: $[PO_4^{3-}]$ ratios were well below Redfield stoichiometry (N:P < 1 from 0 to 75 m, Figure S1 in Supporting Information S1). PO_4^{3-}, $NO_3^- + NO_2^-$, and $[NO_3^- + NO_2^-]$: $[PO_4^{3-}]$ ratios in the upper 75 m were generally within the previous monthly range observed at Station ALOHA, with the exception of $NO_3^- + NO_2^-$ and $[NO_3^- + NO_2^-]$: $[PO_4^{3-}]$ in the 2018 cruise, which approached the maximum values of previous observations (Figure S1 in Supporting Information S1). In both cyclonic eddies, PO_4^{3-} and $NO_3^- + NO_2^-$ concentrations in the lower euphotic zone were among the highest values observed at Station ALOHA (Figure S1 in Supporting Information S1).

Dissolved Fe concentrations ranged from 0.06 to 1.36 nmol L^{-1} within the upper 150 m across all eddies (Figure 2). Concentrations were typically highest at the surface and decreased with depth into the lower euphotic zone; in the 2017 cyclone, dFe concentrations reached a minimum near the DCM and increased in deeper waters alongside the increase in macronutrients (Hawco et al., 2021). In the 2018 anticyclone, dFe concentrations did not vary within the upper 150 m, consistent with the deeper mixed layer and downwelling of surface waters in this eddy. Concentrations were generally higher in the 2018 cruise than in the 2017 cruise, and near-surface dFe patterns between eddies also varied on the two cruises. During the 2017 cruise, dFe in the upper 45 m ranged from 0.17 to 0.31 nmol L^{-1} and were slightly higher in the anticyclone (0.30 ± 0.08 nmol L^{-1}) than in the cyclone (0.23 ± 0.06 nmol L^{-1}). During the 2018 cruise, elevated dFe concentrations were observed in the mixed layer of the cyclone (1.24 ± 0.11 nmol L^{-1} in the upper 45 m), but not in the anticyclone (0.39 nmol L^{-1} at 40 m, within the mixed layer). dFe concentrations greater than 1 nmol L^{-1} in the 2018 cyclone are anomalously high compared to the existing measurements for Station ALOHA (typically between 0.2 and 0.5 nmol L^{-1} in the mixed layer (Fitzsimmons et al., 2015)). In the weeks prior to sampling, the path of the 2018 cyclonic eddy deflected off the northern coast of Maui, possibly leading to input of dFe from coastal sources along the Hawaiian Islands.

3.1.2. N_2 Fixation Rates and Diazotroph Abundances

We measured NFRs using in situ arrays deployed for 24 hr in each eddy center. The highest NFRs were observed in the anticyclones during both cruises, with the highest rates occurring in the 2017 anticyclone (up to 18.6 nmol N L^{-1} d^{-1}, Figure 3). There were strong differences in NFRs between eddies sampled during the 2017 cruise: depth-integrated rates (0–125 m) were ∼6 times higher in the anticyclonic eddy (670 μmol N m^{-2} d^{-1}) than in the cyclonic eddy (115 μmol N m^{-2} d^{-1}). During the 2018 cruise, depth-integrated NFRs were ∼1.7-fold higher in the anticyclone (428 μmol N m^{-2} d^{-1}) than in the cyclone (240–267 μmol N m^{-2} d^{-1}) (Figure 2). In all four sampled eddies, NFRs were highest at the surface and decreased with depth.

We estimated diazotroph abundances by quantifying the *nifH* genes of seven cyanobacterial taxa and by enumerating *Trichodesmium*, *Calothrix*, *Richelia*, and *Crocosphaera* cells/filaments using automated flow cytometry. Depth profiles of *nifH* gene abundances were measured in eddy centers (Figure 3, Table 1, Table S4 in Supporting Information S2) and along a high-resolution sampling transect spanning the two eddies during the 2017 cruise (Figure 4). Automated flow cytometry cell counts were measured continuously in the surface layer, and four consecutive samples (∼2 hr sampling time) corresponding to the nearest *nifH* samples were binned to provide estimates of cell abundances in eddy centers (Table 1). Together, the *nifH* gene- and cell-based datasets indicate that the small diazotrophs UCYN-A and UCYN-B (*Crocosphaera*) were numerically dominant over large diazotroph taxa in all sampled eddies.

During the 2017 cruise, *nifH* gene abundances of UCYN-A (up to 1.4×10^6 *nifH* genes L^{-1}) and UCYN-B (up to 6.2×10^5 *nifH* genes L^{-1}) were higher in the anticyclone center than in the cyclone center (Table 1, Figure 3). Independent measurements of *Crocosphaera* cells via flow cytometry in samples collected within 2 hr of NFR arrays likewise showed higher average concentrations in the anticyclone (4.3×10^5 cells L^{-1}) than in the cyclone (1.92×10^5 cells L^{-1}) and included the presence of both small and large sub-populations (Table 1). Abundances of other taxa were lower (maximum 5.1×10^3 *nifH* genes L^{-1} and 2.2×10^3 cells L^{-1} in surface waters of eddy centers, Table 1) and did not differ between eddies, except for Het-3, which had higher abundances in the cyclone than in the anticyclone. Abundances of most groups decreased with depth, although UCYN-A, UCYN-B, UCYN-C, Het-2, and Het-3 all displayed subsurface maxima (Figure 3, Table S4 in Supporting Information S2).

On the transect spanning the two 2017 eddies, large and small diazotroph taxa displayed different spatial patterns relative to isopycnal displacements (Figure 4). Abundances of *Trichodesmium* and Het-1&2 (symbionts of diatoms) were maximal in surface waters on the northern edge of the anticyclone and in surface waters on the cyclonic side of the front separating the two eddies, where a visual bloom of *Trichodesmium* was also observed (Figure 4). Bucket samples were analyzed with the IFCb to measure the concentration of filaments at the bloom location (148 ± 44 filaments mL^{-1}). Het-3 abundances were highest in subsurface (45 m) waters of the cyclonic eddy just above the 24.5 kg m^{-3} isopycnal. In contrast, abundances of UCYN-B and UCYN-A were highest in the anticyclonic eddy, with maximal abundances from 15 to 45 m for UCYN-B and 45–75 m for UCYN-A (Figure 4).

During the 2018 cruise, UCYN-A had the highest *nifH* gene abundances of all groups quantified (maximum abundance of 6.2×10^5 *nifH* genes L^{-1}, Table 1). UCYN-A abundances within the upper 75 m did not vary between eddy centers, while in the lower euphotic zone (100–125 m), abundances decreased, but were higher in

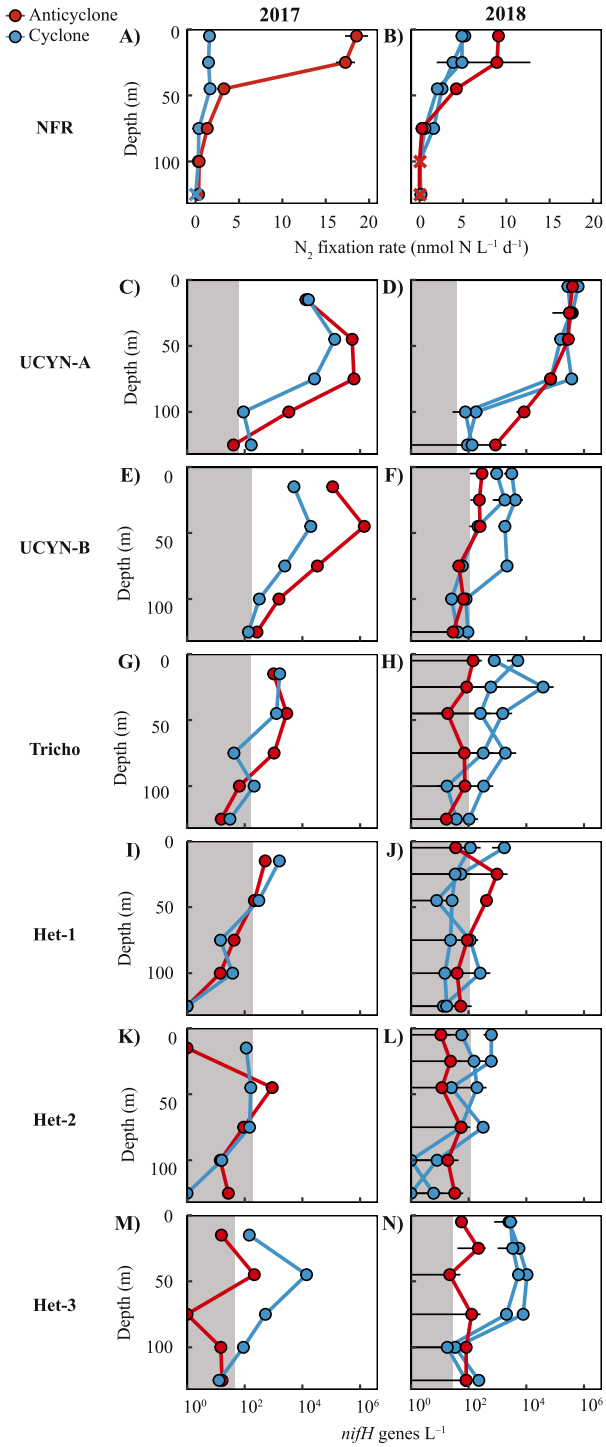

Figure 3. N_2 fixation rates (NFRs, A-B, linear scale) and *nifH* gene abundances (C-N, log-scale) measured in the center of eddies during the 2017 (left) and 2018 (right) cruises. Note that NFR and *nifH* gene abundances were measured twice within the 2018 cyclone. × represent rates below detection limits; shaded areas indicate the detection limits of each digital droplet polymerase chain reaction (ddPCR) assay. Error bars represent the standard deviation among biological replicates ($n = 3$ for NFR data, $n = 2$ for 2018 ddPCR data, not available for 2017 ddPCR data). *nifH* gene abundances of UCYN-C were relatively low (maximum 2.2×10^4 L^{-1}) and are not presented here; they can be found in Table S4 in Supporting Information S2.

the anticyclone ($4.6 \times 10^3 \pm 5.6 \times 10^3$ *nifH* genes L^{-1}) than in the cyclone ($1.2 \times 10^2 \pm 4.7 \times 10^1$ *nifH* genes L^{-1}) (Figure 3). Abundances of other groups were lower (maximum 3.8×10^4 *nifH* genes L^{-1} and 1.9×10^3 cells L^{-1} in surface waters of eddy centers, Table 1) and generally decreased with depth (Figure 3). *nifH* gene abundances of Het-1 did not display consistent differences between eddies (Figure 3, Table S4 in Supporting Information S2). In comparison, *nifH* gene abundances of UCYN-B, UCYN-C, *Trichodesmium*, Het-2, and Het-3 were all generally higher in the cyclonic eddy than in the anticyclonic eddy, despite higher NFRs in the latter. IFCb cell count data likewise show that during the 2018 cruise, *Trichodesmium* and DDAs were more abundant in the cyclone than in the anticyclone and that abundances of all groups were generally lower than in the 2017 cruise. Notably, all *Crocosphaera* cells belonged exclusively to the large-size phenotype and *Calothrix* was mainly found free-living and not attached to their diatom hosts.

3.2. Growth and Grazing of Diazotrophs at the Mesoscale

We investigated potential bottom-up and top-down controls on diazotroph populations to understand the mechanisms driving observed differences in abundances and NFRs between eddies. Bottom-up control mechanisms were explored by modeling diazotroph growth rates as a function of limiting factors (Section 4.2.1) and examining patterns in diazotroph P- and Fe-stress marker gene expression in eddies (Section 4.2.2). Top-down controls were explored by comparing the community structure of putative diazotroph grazers and modeled grazing rates among the sampled eddies (Section 4.2.3).

3.2.1. Modeled Diazotroph Growth Rates and Limiting Factors

Diazotroph growth rates and the factors limiting growth were predicted for the euphotic zone along eddy transects. This was accomplished using a physiological model forced with mean in situ PAR, temperature, PO_4^{3-}, and dFe concentrations and parameterized using taxa-specific ecophysiological parameters gleaned from culture and modeling studies in the existing literature (Table S3 Supporting Information S1). Due to their dependence on light and/or temperature, growth rate predictions were generally higher within the mixed layer and decreased with depth, with the exception of DDAs, for which the effect of temperature has not been tested in cultures (Text S2 in Supporting Information S1). Growth rates of UCYN-A could not be modeled due to a lack of available culture data and growth parameterization. In general, the compilation of growth parameters highlighted large differences in theoretical maximum growth rates among taxa, with values of 0.91 d^{-1}, 0.6 d^{-1}, 0.26 d^{-1}, and 0.33 d^{-1} for large-size *Crocosphaera*, *Richelia*, *Calothrix*, and *Trichodesmium*, respectively (Table S3 in Supporting Information S2). Growth rate predictions across eddy transects were always highest for *Crocosphaera*, with maximum rates of 0.58 ± 0.18 d^{-1} and 0.28 ± 0.13 d^{-1} within the mixed layer in 2017 and 2018, respectively (Figures 5a and 5g, Table 2). *Trichodesmium* appeared to grow at rates that were near its theoretical maximum in 2017 (0.24–0.25 d^{-1}) and at slower rates in 2018 presumably due to lower observed temperatures (Figures 2, 5k, and 5l). In contrast, predictions for DDAs were consistently lower than their theoretical maximum, with maximum growth rates of 0.16 d^{-1} and 0.07 d^{-1} for *Richelia* and *Calothrix*, respectively. Diatom-diazotroph association growth rates were generally higher in 2018, when nutrient concentrations were elevated, and at depths of ~50–75 m in 2017, when subsurface nutrient concentrations were well above that of the stratified surface layer (Figure 2).

Table 1
Average nifH Gene (Genes L^{-1}) and Cell Abundances (Cells L^{-1}) of Diazotroph Taxa Measured by Digital Droplet Polymerase Chain Reaction (15 m for 2017 Cruise; 25 m for 2018 Cruise) and Automated Flow Cytometry (7 m) in Eddy Centers

		Crocosphaera (UCYN-B)					
	UCYN-A	(Small-size class)	(Large-size class)	*Trichodesmium*	*Richelia* (*Het*-1&2)	*Calothrix* (*Het*-3)	Units
2017 Anticyclone							
transect	1.3×10^4	1.1×10^5		1.0×10^3	5.1×10^2	BD	genes L^{-1}
	NA	(2.1×10^5)	(2.9×10^4)	2.2×10^3	6.3×10^2	BD	cells L^{-1}
NFR array	NA	(3.7×10^5)	(5.8×10^4)	BD	2.7×10^3	1.3×10^2	cells L^{-1}
2017 Cyclone							
transect	1.6×10^4	5.1×10^3		1.6×10^3	1.7×10^3	1.4×10^2	genes L^{-1}
	NA	(1.2×10^5)	(8.9×10^2)	1.5×10^3	6.9×10^2	1.4×10^2	cells L^{-1}
NFR array	NA	(9.2×10^3)	(1.0×10^4)	4.8×10^3	1.1×10^3	5.8×10^2	cells L^{-1}
2018 Anticyclone							
	3.1×10^5	2.4×10^2		8.5×10^1	9.9×10^2	2.2×10^2	genes L^{-1}
	NA	(BD)	(2.2×10^2)	BD	BD	2.5×10^2	cells L^{-1}
2018 Cyclone							
Array 1	3.9×10^5	4.2×10^3		5.9×10^2	6.6×10^2	5.6×10^3	genes L^{-1}
	NA	(BD)	(BD)	7.1×10^2	2.7×10^2	1.9×10^3	cells L^{-1}
Array 2	3.4×10^5	1.8×10^3		3.8×10^4	1.9×10^2	3.4×10^3	genes L^{-1}
	NA	(BD)	(9.3×10^2)	2.2×10^2	BD	1.6×10^3	cells L^{-1}

Note. Surface abundances measured by flow cytometry within 2 hr of the sampling time of the NFR arrays in 2017 are also shown. NA: data not available. BD: below detection limits.

Predicted dominant limiting factors varied among taxa and between sampling periods (Figures 5d–5f, 5j–5l). Given the relatively low affinity of *Crocosphaera* for PO_4^{3-} ($k_{PO_4^{3-}} = 18.1 \pm 4.9$ nmol L^{-1}) and the large differences in surface concentrations observed in 2017 (Figure 2), predicted surface growth rates (≤50 m) appeared PO_4^{3-}-limited in the cyclone and not limited by any factor in the anticyclone (based on a limitation threshold equivalent to 2/3 of the maximum theoretical growth rate). Consequently, predicted *Crocosphaera* growth rates were significantly higher in the 2017 anticyclone (0.58 ± 0.18 d^{-1}) than in the 2017 cyclone (0.49 ± 0.11 d^{-1}). This represents the only significant difference in predicted surface growth rates between eddies across all taxa examined according to the weighted generalized linear model, which assumes that rates follow a quasi-binomial distribution (p-value: 7.9×10^{-5}, Table 2). Surface predictions were similar across eddies for *Trichodesmium*, which appeared non-limited at the surface and equally limited by dFe below 50 m, and *Richelia/Calothrix*, which appeared PO_4^{3-} -limited at the surface (≤50 m) and dFe-limited at depth (≥75 m) in both eddy centers. In 2018, the dominant limiting factors for *Crocosphaera* and *Trichodesmium* were predicted to be temperature above 100 m and PAR at deeper depths. None of the surface or deep growth rate estimates differed between eddies, as all abiotic factors examined remained similar in the cyclone and anticyclone (Figure 2). DDAs were predicted to be PO_4^{3-}-limited throughout the water column, except near 100 m in the cyclone, where higher PO_4^{3-} concentrations led to light-limitation (Figure 2).

3.2.2. Diazotroph Expression of P- and Fe-Stress Marker Genes

We analyzed patterns of diazotroph expression of known P- and Fe-stress marker genes using metatranscriptomes collected within the mixed layer and DCM during the 2017 cruise. Transcripts of six P-stress genes and three Fe-stress genes were detected for *Crocosphaera* in surface waters (Figure 6). Fewer gene transcripts were detected for *Trichodesmium* and *Richelia* in surface waters, and transcript abundance for all these diazotrophic cyanobacterial groups was minimal at the DCM, as expected given their lower abundances (Figure 6). No genes examined in UCYN-A or *Calothrix* had transcript levels above detection limits. *Crocosphaera* transcript abundances of all six P-stress marker genes were significantly higher within the mixed layer of the cyclonic eddy,

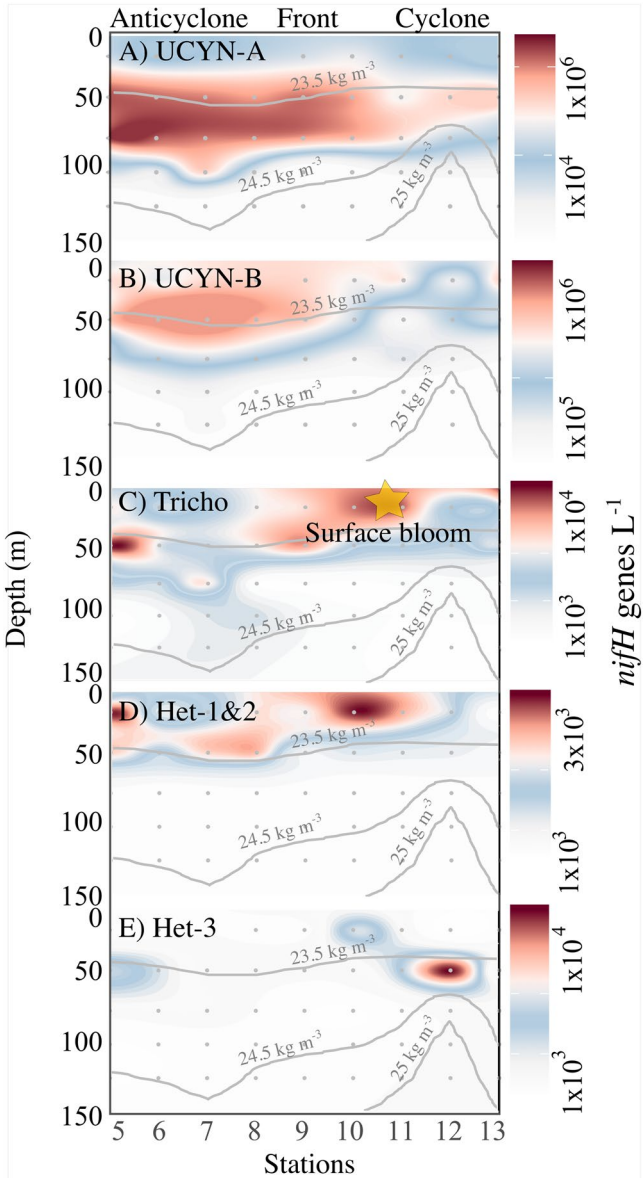

Figure 4. Interpolated *nifH* gene abundances of UCYN-A (a), UCYN-B (*Crocosphaera*, b), Tricho (*Trichodesmium*, c), Het-1&2 (*Richelia*, d), and Het-3 (*Calothrix*, e) across the high resolution 2017 eddy transect. The contours of potential density anomaly (kg m^{-3}) in A-E depict the vertical displacement of isopycnal surfaces associated with mesoscale eddies. A surface bloom of *Trichodesmium* (yellow star, positioned in the contour based on its latitude between Stations 10 and 11) was visually detected and sampled with imaging flow cytometry.

where PO_4^{3-} concentrations were significantly lower (Figure 2), as compared to the anticyclonic eddy (Figure 6). Transcripts for two *Richelia* P-stress genes were detected at the surface: the sulfolipid biosynthase (*sqdB*) abundances were significantly higher in the cyclonic eddy, while the high-affinity phosphate transporter (*pstS*) abundances did not differ between eddies. The only *Trichodesmium* P-stress gene transcript detected, a phosphonate transporter (*phnE*), did not differ in abundance between eddies.

Of the three *Crocosphaera* Fe-stress genes with transcripts detected in the mixed layer, only one (*feoB*, related to Fe(II) acquisition/transport) had higher transcript levels in the cyclonic eddy (Figure 6g). The other two detected gene transcripts (*idiA*, the putative periplasmic Fe(III) binding protein, and *isiA*, encoding the iron-free electron transfer protein flavodoxin) had no significant difference in transcript abundance between eddies (Figures 6g and 6j). The only additional diazotroph Fe-stress gene transcript detected was the iron deficiency-induced protein (*idiA*) gene for *Trichodesmium*, which had no significant difference in abundance between eddies (Figures 6h and 6k).

3.2.3. Diazotroph Grazer Community Structure and Estimated Grazing Rates

We identified diazotroph grazers by analyzing protists co-occurring with *Crocosphaera*, *Trichodesmium*, or DDAs (time-series and fit shown in Figure S3 in Supporting Information S1), and via microscopic visual evidence of diazotroph ingestion in IFCb images (Figure 7). Putative grazers with significant interaction with specific diazotrophs (Figure S2a in Supporting Information S1) included the dinoflagellates *Gymnodinium*, *Cochlodinium*, *Protoperidinium*, *Katodinium*, and *Prorocentrum*, the ciliates *Strombidium* and *Uronema*, and large copepods and nauplii, most of which were imaged with ingested diazotrophs during the eddy cruises (Figures 7a–7i). Results of a predator-prey model provide estimates of grazing rates on specific diazotrophs, corresponding to the rate of their consumption by putative grazers, during the two eddy cruises (Figures 7j and 7k). The grazing rates of copepods were not accounted for in this analysis as their low abundance (8 ± 3 cells L^{-1} in 2017 and 1.6 cells L^{-1} in 2018) precluded the predator-prey model from accurately estimating grazing rates (Text S3 in Supporting Information S1). Also, grazing by small protists (<4 μm) or upon small diazotrophs (<4 μm, including UCYN-A) could not be assessed using this method due to the size constraints of IFCb imaging.

According to the predator-prey model, maximum grazing rates on an individual diazotroph taxon ranged from 0.08 to 0.23 d^{-1} for heterotrophic dinoflagellates, 0.12–0.22 d^{-1} for mixotrophic dinoflagellates, and 0.02–0.16 d^{-1} for ciliates (Figures 7j and 7k). Patterns in grazing rates and sequences (ribotags) from near the V4 region of the 18S rRNA gene from metatranscriptomes (methods and results described in Text S5 in Supporting Information S1) may be difficult to uncover as they are driven by differences in both grazer activities and abundances. However, predicted grazing rates varied between eddies for most putative grazers, with the exception of *Cochlodinium*, *Katodinium*, and *Gyrodinium*, whose apparent abundances determined by the IFCb and metatranscriptome sequencing showed no significant differences or inconsistent patterns between eddies of opposite polarity (Figures 7j and 7k, Text S5 in Supporting Information S1). These dinoflagellates were identified as putative grazers of the large/endosymbiotic diazotroph *Richelia*, whose overall predicted grazing rates were always below 0.1 d^{-1}, resulting in similar predicted grazing pressure (the ratio of predicted grazing rate to growth rate) of 81 ± 9% in cyclones and 69 ± 75% in anticyclones (Table 2). In comparison, our results based on the dynamics of *Crocosphaera* and *Calothrix* show that their putative predators displayed higher grazing rates, and resulting pressure in eddies of specific polarity in both 2017 and 2018.

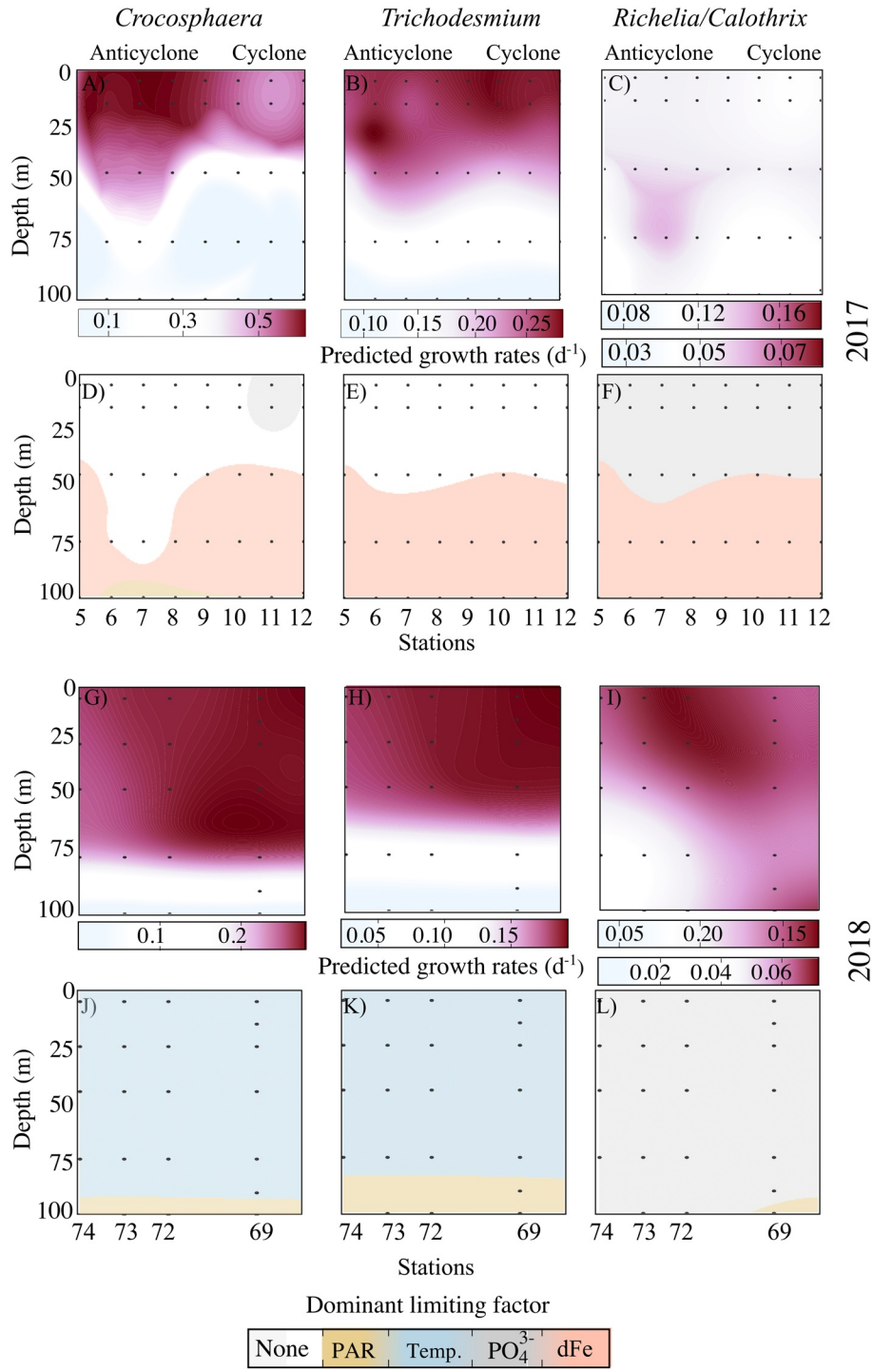

Figure 5. Estimates of the growth rates and limiting factors for *Crocosphaera* (a, d, g, j), *Trichodesmium* (b, e, h, k), and *Richelia/Calothrix* (c, f, i, l) in eddy cruises. Predictions of growth rates (a–c, g–i) and limiting factors (d–f, j–l) across the eddy transect are based on parameters provided in Table S3 in Supporting Information S1 combined with interpolated cross-sections of temperature (Temp.), average scalar irradiance (PAR), and inorganic nutrient concentrations (PO_4^{3-}, dFe). Since parameters for limiting resources were identical for *Richelia* and *Calothrix*, with the exception of respective maximum growth rates reflected in the top (*Richelia*) and bottom (*Calothrix*) scales, predictions showed similar patterns. The locations of the observations with the lowest resolution (nutrient concentrations) are indicated by the black dots.

Table 2
Predictions of Diazotroph Biological Rates in Eddy Centers During the 2017 and 2018 Cruises

Eddy	Rates (d^{-1})	*Crocosphaera*	*Trichodesmium*	*Richelia*	*Calothrix*
2017:	*p*-value	$7.9 \times 10^{-5***}$	$0.22^{\dagger}$	$0.1^{\dagger}$	$0.11^{\dagger}$
	$\mu(T,E,PO_4^{3-},dFe)$	0.49 ± 0.11	0.25 ± 0.08	0.09 ± 0.05	0.04 ± 0.01
Cyclone	*r*	0.24 ± 0.06	0.18 ± 0.03	0.12 ± 0.05	0.11 ± 0.07
	g	0.50 ± 0.14	NA	0.08 ± 0.02	0.02 ± 0.01
	g:μ (%)	102 ± 48	NA	88 ± 80	50 ± 75
Anticyclone	$\mu(T,E,PO_4^{3-},dFe)$	0.58 ± 0.18	0.24 ± 0.03	0.13 ± 0.04	0.05 ± 0.02
	r	0.42 ± 0.10	0.16 ± 0.01	0.16 ± 0.04	0.15 ± 0.10
	g	0.39 ± 0.11	NA	0.09 ± 0.04	0.18 ± 0.03
	g:μ (%)	67 ± 59	NA	69 ± 75	360 ± 57
2018:	*p*-value	$0.22^{\dagger}$	$0.08^{\dagger}$	$1^{\dagger}$	$1^{\dagger}$
	$\mu(T,E,PO_4^{3-},dFe)$	0.28 ± 0.13	0.19 ± 0.07	0.16 ± 0.06	0.07 ± 0.03
Cyclone	*r*	0.19 ± 0.60	0.09 ± 0.00	0.06 ± 0.01	0.18 ± 0.06
	g	0.40 ± 0.16	NA	0.12 ± 0.02	0.04 ± 0.01
	g:μ (%)	142 ± 61	NA	75 ± 41	57 ± 49
Anticyclone	$\mu(T,E,PO_4^{3-},dFe)$	0.26 ± 0.12	0.18 ± 0.06	0.14 ± 0.06	0.06 ± 0.03
	r	0.26 ± 0.10	0.002 ± 0.001	0.02 ± 0.00	0.20 ± 0.07
	g	0.24 ± 0.09	NA	NA	0.10 ± 0.01
	g:μ (%)	92 ± 59	NA	NA	166 ± 50

Note. Biological rates were derived from population models applied to diazotrophs imaged by the IFCb (large *Crocosphaera*, *Trichodesmium*, *Richelia*, and *Calothrix*). Intrinsic growth rates, μ(T,E, PO_4^{3-},dFe), were predicted across the euphotic zone based on culture adaptations to temperature (T), instantaneous light (E), phosphate (PO_4^{3-}) concentration, and dissolved iron (dFe) concentration (Figure 5). *P*-values are reported to assess whether growth rates were significantly different in eddies of opposite polarity. Here, we report growth rate predictions (μ(T,E, PO_4^{3-},dFe) ± standard deviation derived from the uncertainty of parameters using the R package propagate) matching estimates of surface (7 m) diazotroph growth rates (r ± standard deviation) and grazing rates (g ± standard deviation) based on Lagrangian time-series of diazotroph and protistan populations. The grazing pressure (g:μ) is reported to indicate whether a diazotroph population grew faster than it was grazed upon ($g < \mu$), allowing for potential accumulation. Note that r is generally lower than the intrinsic growth rates μ(T,E, PO_4^{3-},dFe), as this parameter accounts for additional losses from other grazers, viruses, programmed cell death, vertical migration, and/or sinking. NA: Not Available, *P*-values: *** (<0.001) † (not significant).

A few taxa consumed *Crocosphaera* or DDAs at higher predicted rates in cyclones, including *Gymnodinium* (0.12 ± 0.04 d^{-1} in the cyclone and 0.001 ± 0.04 d^{-1} in the anticyclone) and *Prorocentrum* (0.18 ± 0.06 d^{-1} in the cyclone and 0.05 ± 0.06 d^{-1} in the anticyclone). Both taxa had higher ribotag signals in the 2017 cyclone (Figure S5 in Supporting Information S1). Likewise, their abundances generally increased by 29 ± 10% and 15 ± 15% respectively in cyclones, with both dinoflagellates being more abundant in the summertime. IFCb analysis indicated that these appeared to graze mainly upon *Crocosphaera* ($R^2 = 0.71$ and 0.32 in 2017 and 2018, respectively), with a mean predicted grazing pressure 53 ± 1% higher in cyclonic eddies than in anticyclonic eddies (Table 2). Grazing pressure was predicted to be above 100% in both cyclones, suggesting that the majority of new *Crocosphaera* cells produced by division were grazed upon, with conversely lower percentages in the anticyclones. These results are consistent with the gradual increase in *Crocosphaera* cell abundances measured in the center of the anticyclone in 2017, and quasi steady-state dynamics observed otherwise (Figure S3 in Supporting Information S1).

Conversely, grazers responsible for higher putative grazing upon diazotrophs in anticyclones included *Protoperidinium* (0.20 ± 0.04 d^{-1} in the anticyclone and 0.004 ± 0.006 d^{-1} in the cyclone), whose ribotags were also significantly more abundant in the 2017 anticyclone (Figure S5 in Supporting Information S1), *Gyrodinium* (0.05 ± 0.06 d^{-1} in the anticyclone and 0.02 ± 0.03 d^{-1} in the cyclone), and *Amphidinium* (0.07 ± 0.004 d^{-1} in the anticyclone and 0.007 ± 0.01 d^{-1} in the cyclone). Likewise, these taxa had higher abundances in anticyclones than in cyclones (73 ± 42%, 38 ± 3%, and 21 ± 22% higher on average respectively), with little variation across years, except for *Gyrodinium*, whose abundances were much higher in 2018 (Figure 7). These grazers were

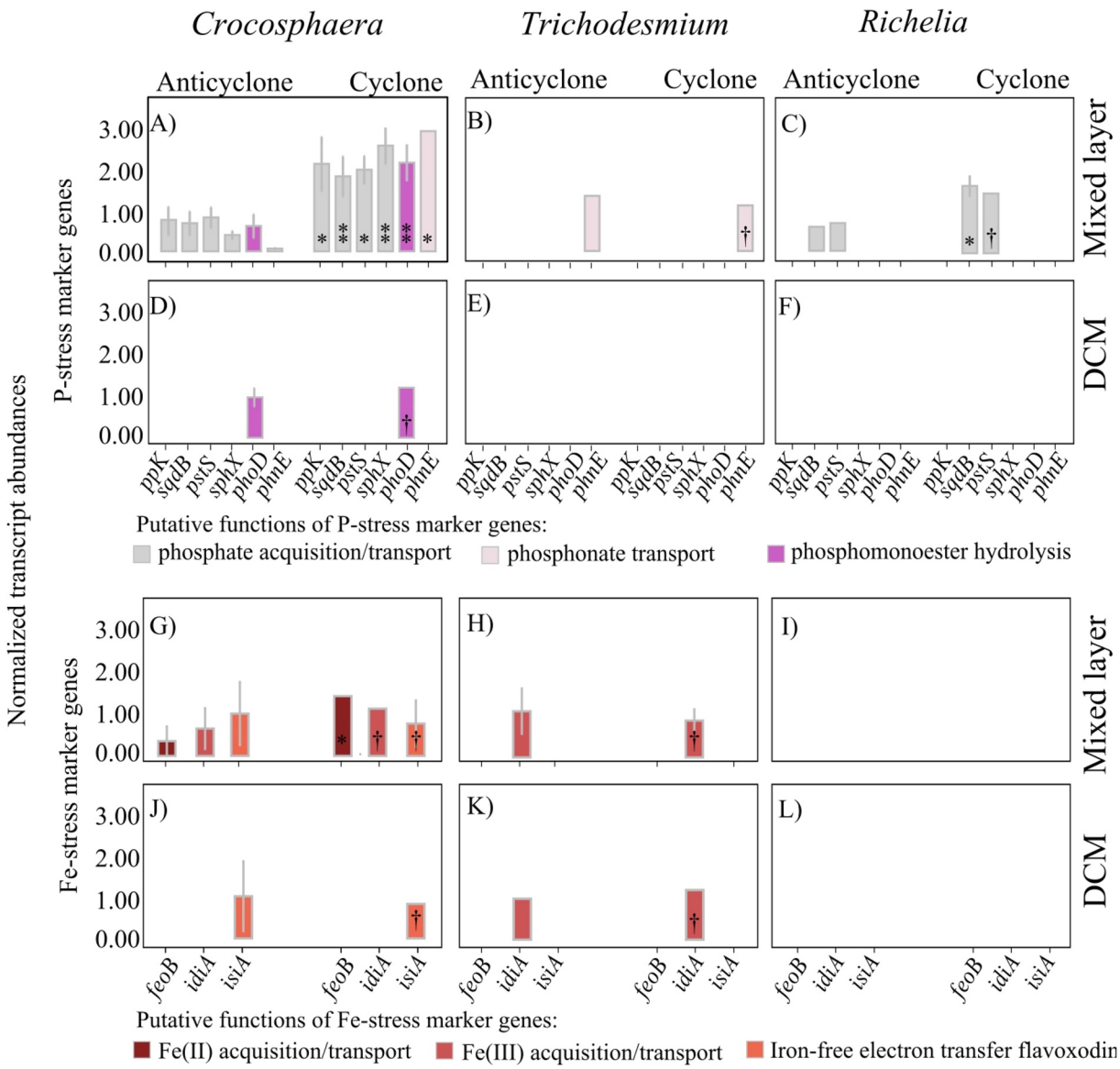

Figure 6. Relative expression of P- (a–f) and Fe-stress (g–l) marker genes (according to Stenegren (2020) and Snow et al. (2015)) of *Crocosphaera*, *Trichodesmium*, and *Richelia* within the mixed layer (15 m) and at the deep chlorophyll maximum (DCM) in 2017. Individual bars represent the average (± standard errors) standardized transcript abundances for each stress marker gene in a specific eddy. P-stress markers include genes related to dissolved inorganic (*ppk*: *polyphosphate kinase*, *sqdB*: *sulfolipid biosynthase (substitution of P-lipids)*, *pstS/sphX*: *high-affinity phosphate transporter*) and organic (*phoD*: *Alkaline phosphatase*, *phnE*: *phosphonate transporter*) P acquisition/transport. Fe-stress markers include genes related to dissolved inorganic iron acquisition/transport (*feoB*: *ferrous iron transporter*, *idiA*: *iron deficiency-induced protein*) and the substitution of enzymes involved in electron transport (*isiA*: *flavodoxin*). *P*-values: ** (<0.005) * (<0.01) † (not significant).

associated with a high predicted grazing pressure upon *Calothrix* in anticyclonic eddies (mean 263 ± 137%, Table 2), reflected in the progressive decrease in filaments imaged with the IFCb with model R^2 of 0.4 and 0.73 in 2017 and 2018, respectively (Figure S3 in Supporting Information S1).

4. Discussion

4.1. NFRs and Diazotroph Abundances at the Mesoscale

Mesoscale eddies add variability to the biogeochemistry and microbial community structure in the NPSG (Barone et al., 2019; Barone et al., 2022), but the effects of eddies on N_2 fixation are not fully understood. We sampled two pairs of eddies in spatial proximity, providing a unique opportunity to explore the effects of anticyclonic and

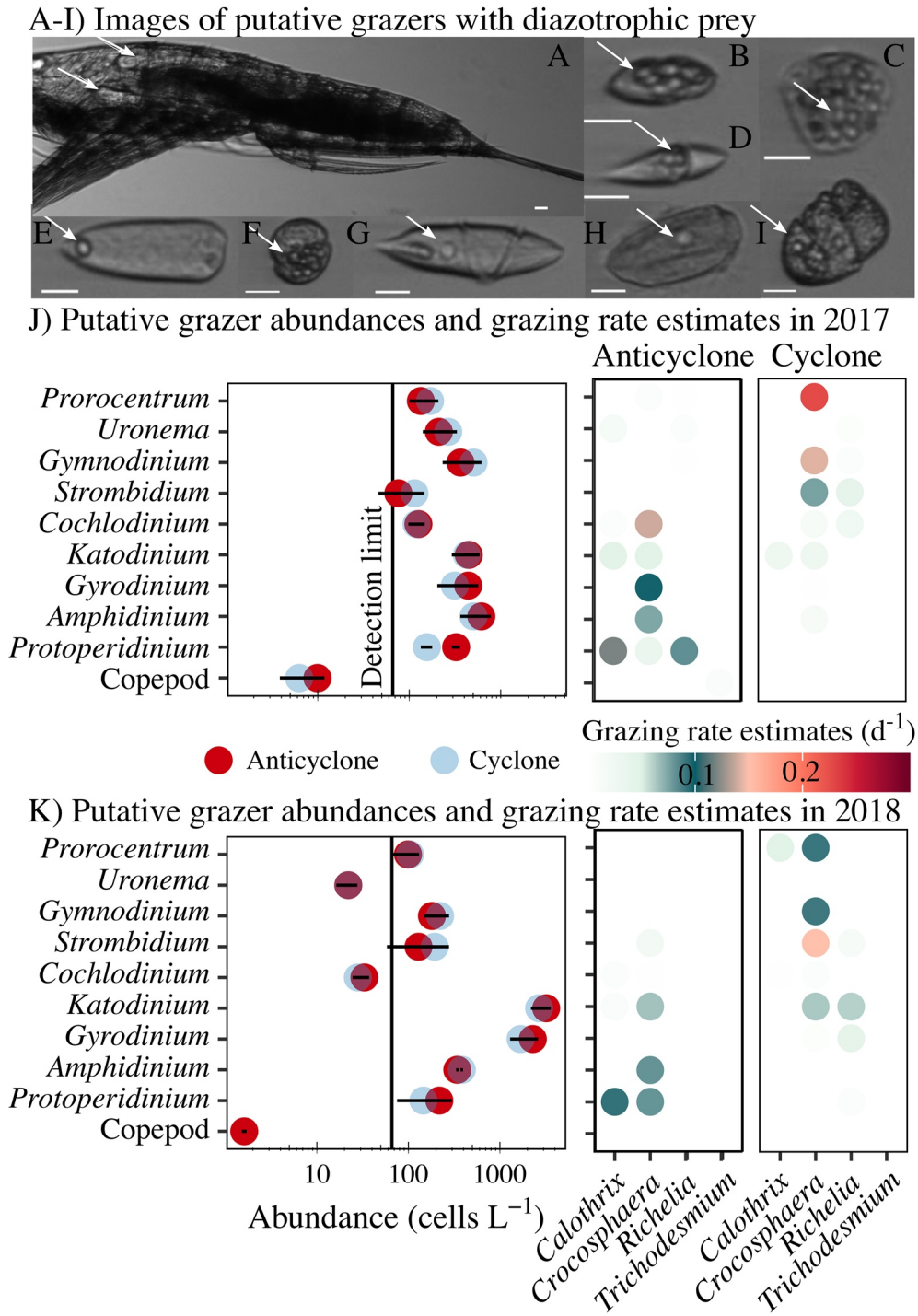

Figure 7. Evidence of grazing upon diazotrophs in eddy cruises from images of co-occurring protists with ingested prey (a)–i) and grazing rate estimates based on predator-prey dynamics (j, k). Grazing rates were predicted from diazotroph and protist abundances (Figure S3 in Supporting Information S1) and interaction coefficients (*p*-values shown in Figure S2b in Supporting Information S1). Patterns across eddies of opposite polarities were generally consistent for both putative grazer abundances and grazing rate estimates. Diazotrophic prey (indicated by arrows) were imaged inside copepods/nauplii (a), *Katodinium* (b), *Strombidium* (c), *Amphidinium* (d), *Prorocentrum* (e), *Gymnodinium* (f), *Gyrodinium* (h), *Uronema* (i), and *Cochlodinium* (j). Scale bars: 10 μm.

cyclonic eddies on diazotrophy independent of seasonal changes. Since samples were collected in the vicinity of Station ALOHA, we also leveraged data from the HOT program (Karl & Church, 2014) to provide a historical and a seasonal context to our observations.

NFRs in both anticyclone centers examined here were anomalously high relative to previous measurements at Station ALOHA. Surface (25 m) rates in these eddies exceeded all previous NFRs from the time-series (2012–2019), with values 3.7- and 1.8-fold above the highest previous HOT observations from the months of sampling (July and April, respectively) (Figure 8). Between 2012 and 2019, 13 trackable eddies occupied Station ALOHA during a HOT cruise, yet no NFR measurements from these cruises occurred close to the eddy center (data not shown); hence, it is possible that we observed high NFRs in anticyclones because we specifically targeted the center of mesoscale eddies. In contrast, rates in both cyclones were within the range of previous observations. During the 2017 cruise, the range in depth-integrated NFRs between eddies, sampled 5 days and ∼2° latitude apart, exceeded the range in monthly mean NFRs from the time-series measurements (∼100–400 μmol N m^{-2} d^{-1}, Böttjer et al., 2017). Our results are similar to the studies of Fong et al. (2008) and Wilson et al. (2017), which both sampled anticyclonic eddies in the NPSG during July and observed anomalously high NFRs (surface rates of 8.6 and 10.9 nmol N L^{-1} d^{-1}, respectively). The March-April 2018 cruise data also highlights that elevated NFRs in anticyclones are not necessarily restricted to warm (>25°C) summer months, as previously observed by Church et al. (2009).

The high NFRs observed in the 2017 and 2018 anticyclones appear to be driven by different diazotroph taxa. UCYN-A *nifH* gene abundances were the highest of all groups quantified during the spring (2018) cruise and UCYN-A and *Crocosphaera* (UCYN-B) were most abundant in the summer (2017) cruise (Figures 3 and 8). This is consistent with the known seasonal succession of *nifH* gene-based diazotroph abundances at Station ALOHA: abundances of *Trichodesmium*, *Crocosphaera*, and DDA *nifH* genes peak in the summer or early fall, while abundances of UCYN-A peak during the spring (Böttjer et al., 2014; Church et al., 2009). However, our only observation of both anomalously high diazotroph abundances and high anticyclone NFRs was during the 2017 cruise, when *Crocosphaera* abundances in the anticyclone exceeded all previous measurements in the region from the months of June and July (Figure 8). The high abundances of *Crocosphaera* in the 2017 anticyclone were verified by independent cell counts via automated flow cytometry (Table 1). Although UCYN-A abundances were also high in the 2017 anticyclone, they only slightly exceeded the seasonal mean (Figure 8). We infer that *Crocosphaera* likely played a major role in driving the high NFRs observed in the 2017 anticyclone. High *Crocosphaera* abundances have been recently linked to high NFRs in another anticyclonic eddy of the NPSG during July (Wilson et al., 2017).

It is less clear which diazotroph taxa drove the high NFRs observed in the 2018 anticyclone. In 2018, UCYN-A had the highest *nifH* gene abundances of all diazotrophs quantified; however, abundances were near the monthly mean and did not differ between eddies (Figures 3 and 8). No diazotroph taxa quantified via *nifH* gene abundances or automated flow cytometry had higher abundances in the anticyclonic eddy, where the highest rates were measured. There are several possible explanations for this apparent mismatch between diazotroph abundances and NFRs. NFRs vary as a function of both diazotroph abundance and cell-specific activity; hence, the difference in rates between eddies could be due to differences in cell-specific activity rather than abundance. These differences were investigated for known cyanobacterial diazotrophs and are discussed in Section 4.2.1 below. Our ddPCR assays may also miss important diazotrophic taxa, such as non-cyanobacterial diazotrophs, whose importance in marine ecosystems are not well-understood (Moisander et al., 2017), or could misrepresent organismal abundances due to polyploidy (Gradoville et al., 2022; Sargent et al., 2016), low DNA extraction efficiency (Boström et al., 2004), or other methodological biases. Finally, the pattern observed in 2018 may be driven by the patchiness of diazotroph communities (e.g., Robidart et al., 2014). We next examine evidence for eddy modulation of bottom-up, top-down, and physical control on diazotroph abundance and activity to better understand the mechanistic underpinnings of the observed patterns (Section 4.2). Finally, we address the challenges in generalizing the effects of eddies on N_2 fixation due to confounding effects of season, diazotroph community structure, and eddy age/stage (Section 4.3).

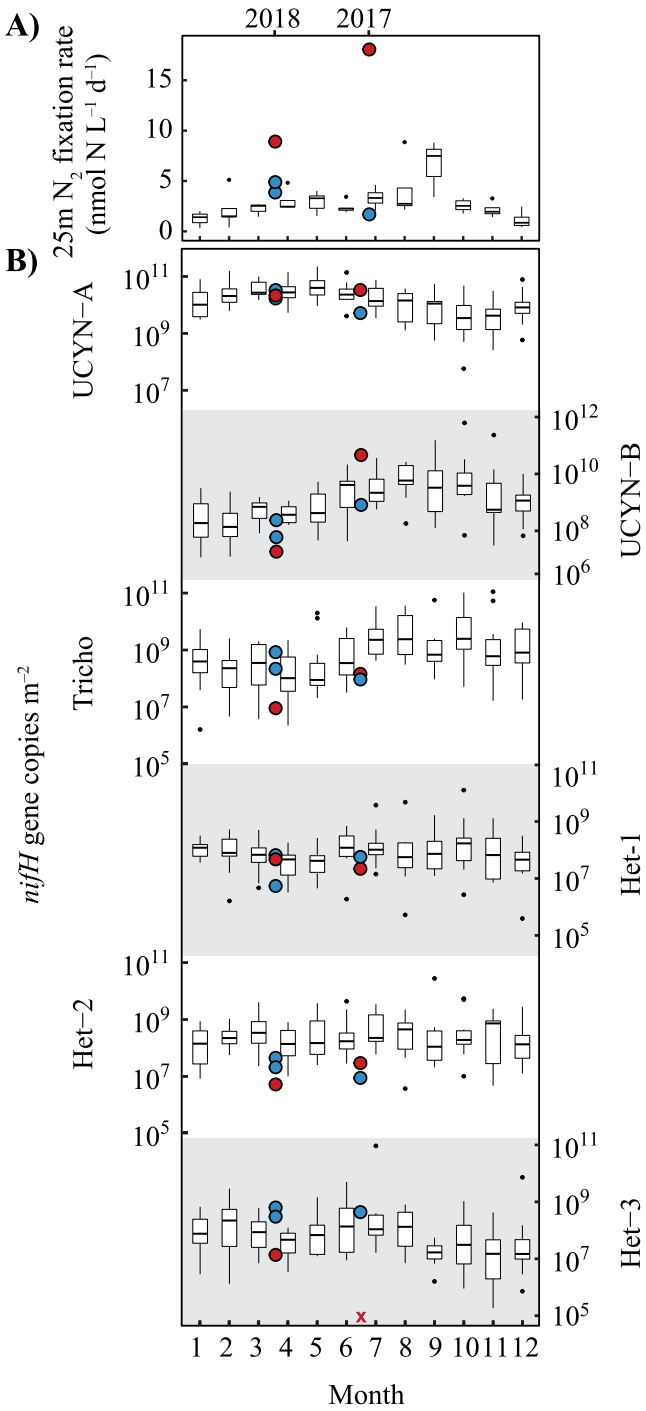

Figure 8. Eddy observations (cyclones [blue] and anticyclones [red]) of N_2 fixation rates at 25 m depth (A, linear scale) and depth-integrated (0–125 m) *nifH* gene abundances (B, log scale) superimposed on historical Hawaii Ocean Time-series data. Boxplots illustrate ~ monthly measurements observed at Station ALOHA from 2012 to 2019 for N_2 fixation (Böttjer et al., 2017) and from 2004 to 2017 for qPCR-derived *nifH* gene abundances (data set https://doi.org/10.5281/zenodo.4477269). Medians are shown as thick horizontal lines, 25%–75% quantiles as boxes, the minimum and maximum values (up to 1.5 times the interquartile range) as whiskers, and outliers as black dots. Observations below detection limits are represented by colored ×. Shading is used to differentiate vertical panels.

4.2. Mechanisms Leading to High NFRs in Anticyclonic Eddies

4.2.1. Bottom-Up Control

Mesoscale eddies can modulate several factors that control diazotroph growth rates. Eddy dynamics can affect sea surface temperature via isopycnal uplift, resulting in cold core cyclones (McGillicuddy & Robinson, 1997) and can affect light attenuation via nutrient injection and subsequent particle formation (Benitez-Nelson et al., 2007). Temperature and light both control cyanobacterial diazotroph growth rates (Table S3 in Supporting Information S1), and global NFRs correlate positively with both parameters (Luo et al., 2014). Eddies also influence nutrient availability (Barone et al., 2022; Hawco et al., 2021). Diazotrophs in the NPSG oscillate between P and Fe limitations (Letelier et al., 2019) and are able to coexist with non-diazotrophic phytoplankton under low N:P and N:Fe supply ratios (Ward et al., 2013). The uplift of isopycnals in cyclonic eddies can inject N, P, and Fe into the lower euphotic zone, where most of these nutrients are rapidly assimilated by the plankton community (McGillicuddy & Robinson, 1997). Conversely, isopycnal downwelling in anticyclonic eddies can result in extreme N-depletion in surface waters, which has previously been used to explain observations of high NFRs in a NPSG anticyclone (Wilson et al., 2017).

In the present study, we employed a suite of techniques that allowed us to address the potential limiting factors of diazotroph growth and modulation by mesoscale physical forcing. We found that the strong differences in NFRs between the anticyclone and cyclone during the 2017 cruise may be partially driven by differences in PO_4^{3-} availability. Surface PO_4^{3-} concentrations and NFRs were significantly higher in the anticyclonic eddy than in the cyclonic eddy (Figure 2). This finding is consistent with a recent analysis of long-term trends at Station ALOHA documenting higher surface PO_4^{3-} concentrations in anticyclonic eddies than in cyclonic eddies, an enigmatic pattern for which the driving mechanisms are not fully understood (Barone et al., 2019). In our 2017 (summertime) cruise, surface PO_4^{3-} in both 2017 eddies fell below 50 nmol L^{-1}, the empirical threshold for P-limitation of diazotrophs in the NPSG reported by Letelier et al. (2019), and PO_4^{3-} concentrations in the cyclone were below 30 nmol L^{-1}, an apparent threshold for severe diazotroph P-limitation (Letelier et al., 2019). We hypothesize that the higher PO_4^{3-} in the 2017 anticyclone partially relieved P-limitation, allowing for higher rates of diazotroph growth and N_2 fixation by diazotrophic taxa, specifically *Crocosphaera*.

Eddy-driven reduction in P-limitation in the 2017 anticyclone is further supported by results from our ecophysiological model, patterns in nutrient stress marker gene expression, and previous studies. The ecophysiological model predicted that during the 2017 cruise, *Crocosphaera* was PO_4^{3-}-limited in the cyclone, but not in the anticyclone, driving higher predicted growth rates in the anticyclone (Figure 5). Indeed, in a complementary study that surveyed the 2017 eddies on the same expedition, *Crocosphaera* populations had higher intrinsic growth rates in the anticyclonic eddy than in the cyclonic eddy (Dugenne et al., 2020). Another study from the same 2017 expedition reported lower bulk alkaline phosphatase activity in the 2017 anticyclone (Harke et al., 2021), supporting the postulated reduced P-limitation there.

The metatranscriptome data provide additional evidence that PO_4^{3-} availability helped drive the difference in *Crocosphaera* growth rates between eddies: all six *Crocosphaera* genes related to P acquisition and transport

(commonly used as P-stress markers, Dyhrman & Haley, 2006; Pereira et al., 2016) had lower normalized transcript abundances in the 2017 anticyclone, consistent with a reduction in P-limitation relative to the cyclonic eddy (Figure 6). We view the combined datasets presented here and in previous studies of the 2017 eddies as strong evidence that increased PO_4^{3-} availability resulted in higher *Crocosphaera* growth rates in the anticyclone. This may ultimately help explain the higher *Crocosphaera nifH* gene abundances, biomass, and bulk NFRs observed in the anticyclone relative to the cyclone (Table 1, Figures 3 and 4).

Nutrient concentrations do not appear to explain the difference in NFRs between the 2018 eddies. Surface nutrient concentrations in the 2018 eddies were higher than in the 2017 eddies and did not differ between the cyclone and anticyclone, possibly due to deep mixing in the 2018 anticyclone prior to the time of sampling. Our ecophysiological model predicted that most diazotrophs in 2018 were limited by low temperature, with the exception of DDAs, which could not be resolved because thermal adaptation for this group has not been tested in cultures. While data on the physiological adaptations of UCYN-A in culture are not available, a complementary study by Gradoville et al. (2021), which sampled eddies on the same 2018 expedition as the present study, reported no significant differences in UCYN-A cell-specific NFRs between eddies, suggesting that bottom-up forcing did not differ between the 2018 eddies for this organism.

It is less likely that the differences in NFRs between cyclonic and anticyclonic eddies were driven by light, temperature, or dFe concentrations on either cruise. There were only small differences in near-surface light flux or temperatures between cyclones and anticyclones, except for the 2018 cruise, where lower daily integrated light was observed in the anticyclone due to cloud cover (Figure 2). Since higher NFRs were observed in the eddy with lower light levels, the opposite trend as expected (Luo et al., 2014), it is very unlikely that temperature or light drove the observed differences in NFRs between eddies, though they may help explain observed differences in NFRs between seasons (see Section 4.3) as well as variation in growth rates of distinct taxa (Figure 5). Likewise, based on existing parameterization of Fe-uptake and expression of Fe-stress marker genes, patterns in NFRs between eddies did not appear to be primarily driven by dFe. In the 2018 cruise, surface dFe concentrations were anomalously high in the cyclonic eddy, where lower NFRs were observed. In the 2017 cruise, dFe concentrations were slightly higher in the anticyclone, where rates were higher (Figure 2). However, ecophysiological model results suggest that Fe was less limiting than PO_4^{3-} at the surface for all diazotroph groups on both cruises (Figure 5). In addition, all surface dFe concentrations fell above the hypothesized Fe-limitation threshold for diazotrophs (0.13 nmol L^{-1}), estimated from the empirical P-limitation threshold for diazotrophs in the NPSG (Letelier et al., 2019) coupled to diazotroph cell stoichiometry. There are caveats linked to testing the effect of Fe concentration in culture and extrapolating these experiments to field populations, as described in Text S2 in Supporting Information S1. Nevertheless, expression patterns of Fe-stress marker genes (available for 2017 only) support our model results since most transcripts did not differ between cyclonic and anticyclonic eddies (Figure 6). Collectively, these data are not consistent with an overriding control by Fe on NFR in our experiments.

We cannot exclude the possibility that there are other bottom-up control factors not analyzed here that could have potentially driven differences in diazotroph growth, and ultimately in bulk NFRs, between eddies. For example, some diazotrophs, such as *Trichodesmium*, use dissolved organic P (DOP) in P-depleted environments (Dyhrman et al., 2006; Orchard et al., 2010; White et al., 2010). Growth of symbiotic diazotrophs can also depend on the bottom-up control factors of their hosts, such as silica for the diatom hosts of *Richelia* and *Calothrix*. We did not report concentrations of DOP, silica, or any micronutrients other than dFe in this study due to a lack of data linking growth rates of cultured diazotrophs to the availability of these nutrients. As such, nutrients and micronutrients not assessed in our model could theoretically have driven differences in NFRs. In sum, of the potentially limiting abiotic factors measured, we find the strongest evidence of differential P limitation. While not exhaustive, our combined datasets, along with model results and long-term trends at Station ALOHA (Barone et al., 2019), suggest that P may be the main abiotic factor driving the differences in NFRs in mesoscale eddies of the NPSG.

4.2.2. Top-Down Control

Little is known about the identity of diazotrophic grazers or the extent to which grazing controls diazotroph abundances and NFRs in the NPSG (Landolfi et al., 2021). Early reports identified mesoplanktonic copepods grazing on *Trichodesmium* (Azimuddin et al., 2016; O'Neil et al., 1996; O'Neil, 1998), and later on UCYN-C (Hunt et al., 2016), UCYN-A (Scavotto et al., 2015), UCYN-B, Het-1, and Het-2 (Conroy et al., 2017). Recently, small nano/microplanktonic species (e.g., dinoflagellates and ciliates) were also shown to prey on the large population

of *Crocosphaera* in the NPSG (Dugenne et al., 2020). These small grazers generally dominate the nano/microzooplankton biomass most of the year (Pasulka et al., 2013). The overall lack of available data on grazers of diazotrophs makes it difficult to study top-down controls on these populations. Here, we use a novel combination of observations and model predictions to address this knowledge gap; note that this approach comes with numerous assumptions and caveats (see Section 2.5.2).

Our predator-prey model and direct IFCb images of ingested prey identified putative predators of diazotrophs whose abundance and predicted activity varied between eddies. Putative grazers spanned various sizes, from large copepods and nauplii imaged after having ingested *Trichodesmium* filaments, to nanoplanktonic ciliates and dinoflagellates mostly preying on *Crocosphaera* or *Calothrix*. Predicted grazing rates varied between cyclonic and anticyclonic eddies (Figure 7). Most of the grazers known to be mixotrophs (Jeong et al., 2010), such as *Prorocentrum*, *Gymnodinium*, and *Strombidium*, were more abundant in cyclones, while the heterotrophs *Protoperidinium*, *Amphidinium*, and *Katodinium* had higher abundances in anticyclones. Understanding the drivers of grazer communities at the mesoscale is beyond the scope of this study, but likely involves differences in their own bottom-up (number of available prey, prey concentrations, additional resources like light and/or nutrients for mixotrophs) and/or top-down (abundance and activity of their predator, parasites, viruses) controls. Nevertheless, the differences in grazer abundances we observed resulted in clear differences in predicted grazing rates upon specific diazotrophs in eddies of specific polarity and may help explain the observed patterns in diazotroph abundances and NFRs. During the 2017 cruise, Het-3 (*Calothrix*) *nifH* gene abundances measured within the mixed layer were 2–4 orders of magnitude greater in the cyclone than in the anticyclone (Figure 3), yet predicted growth rates did not differ between eddies (Figure 5). Our predator-prey model predicts that rates of grazing upon *Calothrix* for the 2017 cruise were significantly higher in the anticyclone than the cyclone (Table 2); thus, the observed differences in *Calothrix* abundance between eddies may simply be explained by differences in grazing pressures. In contrast, estimated rates of grazing upon *Crocosphaera* were higher in the cyclonic eddies for both cruises (Table 2). Therefore, the high abundance of *Crocosphaera* in the 2017 anticyclone appears driven by both enhanced growth rates and reduced grazing pressure, which ultimately helped to drive higher bulk NFRs (Figure 3).

Results presented here and in previous studies (Dugenne et al., 2020; Landry et al., 2008; Wilson et al., 2017) show that grazing can be a significant loss term for small unicellular diazotrophs, but less so for larger diazotrophs such as *Richelia* and *Trichodesmium* (Table 2). Indeed, *Trichodesmium* has few known grazers (O'Neil & Roman, 1992), and losses are more often thought to be driven by viral lysis (Mulholland, 2007). While we did not directly assess viral lysis in this study, visual inspection of *Trichodesmium* filaments from the bloom at the edge of the 2017 cyclone (Figure 4) suggests that *Trichodesmium* losses in the bloom may have been driven by programmed cell death or viral lysis (Berman-Frank et al., 2004; Hewson et al., 2004), as a majority of the filaments contained cells which were shrunken or lacking thylakoids, and bloom filaments had significantly lower chlorophyll per cell than filaments imaged within the 2017 eddy centers (Text S4 and Figure S4 in Supporting Information S1). The fraction of dimly fluorescing *Trichodesmium* filaments did not differ between eddies of specific polarity. We interpret this fraction as evidence for senescence, but other sources of diazotroph mortality, including viral lysis and programmed cell death, should be assessed directly in future studies.

4.2.3. Physical Control

Buoyant plankton can be concentrated in areas of surface convergence, where cells are horizontally advected to the site of convergence and then acted upon by the opposing forces of downwelling and upward buoyancy (D'Asaro et al., 2018; Yoder et al., 1994). The buoyancy of diazotrophic taxa varies greatly: smaller diazotrophs (e.g., *Crocosphaera* and *Calothrix-Chaetoceros*) are negatively buoyant and sink (Bach et al., 2012; Tuo, 2015) while large diazotrophs (*Trichodesmium* and *Richelia* associations) can regulate their buoyancy, sometimes becoming positively buoyant and ascending the water column at high rates (Hoppe, 2013; Villareal & Carpenter, 1989; Villareal & Carpenter, 2003; Walsby, 1978). Elevated surface abundances of *Trichodesmium* and *Richelia* have been observed at numerous frontal features (Aldeco-Ramírez et al., 2009; Benavides et al., 2011; Guidi et al., 2012; Yoder et al., 1994), presumably due to frontal downwelling and strong positive cell buoyancy. In mesoscale eddies, downwelling can occur in intensifying anticyclones and weakening cyclones (McGillicuddy, 2016), cyclones under constant wind (Gaube et al., 2015), and at the cyclonic side of eddy fronts (Mahadevan, 2016). The downwelling-induced physical accumulation of cells has been used to

explain the occurrence of surface *Trichodesmium* slicks (Olson et al., 2015) and *Rhizosolenia* mats (Villareal & Carpenter, 1989) in eddies of both polarities.

The fine-scale distribution of diazotrophs across the pair of adjacent eddies measured in 2017 shows evidence for the physical accumulation of *Trichodesmium* and *Richelia* (Figure 4). The highest *nifH* gene abundances of *Trichodesmium* and *Richelia* were observed near the surface at the cyclonic side of the front separating the two eddies, consistent with accumulation via surface downwelling caused by frontal dynamics. A surface bloom of *Trichodesmium* was also visually observed at the cyclonic side of the front, likely also driven by frontal downwelling. These results are consistent with a previous survey of *Trichodesmium* in an eddy dipole of the NPSG, which also reported maximal abundances at the front between eddies (Guidi et al., 2012).

Our observations are insufficient for determining the importance of physical accumulation on NFRs across the full eddy-eddy transect. NFR measurements were conducted in the center of each eddy, but not on the cyclonic side of the eddy-eddy front where *Trichodesmium* and DDAs appeared to be physically accumulated during the 2017 cruise. Thus, while the eddy-induced physical accumulation of large diazotrophs likely explains elevated NFRs and abundances of large diazotrophs in some previous studies (e.g., Fong et al., 2008; Olson et al., 2015), our eddy observations were likely driven by differences in biological control—the balance of bottom-up and top-down control—between eddies.

4.3. Challenges in Generalizing Eddy Effects on Diazotrophs

Our finding of high NFRs in anticyclonic eddies agrees with other recent observations of high NFRs in anticyclones from many ocean regions (Fong et al., 2008; Holl et al., 2007; Liu et al., 2020; Löscher et al., 2016; Rahav et al., 2013; Wilson et al., 2017). However, there have also been reports of high diazotroph abundances associated with cyclonic eddies (Olson et al., 2015), and on a different cruise that sampled a cyclone-anticyclone eddy pair in the NPSG, surface NFRs were significantly higher in the cyclonic eddy than in the anticyclonic eddy (data set https://doi.org/10.5281/zenodo.5565560). At Station ALOHA, the correlation between NFR and SLA measured between 2012 and 2019 has remained non-significant (Spearman correlation, $r = 0.08$, p-value $= 0.58$, $n = 48$, data not shown), yet high rates of N_2 fixation are more prevalent in warm summer months often coincident with high SLA.

Despite this relative predictability, several taxa showed inconsistent patterns with eddy polarity during our cruises. Our data suggest that the effects of eddies vary strongly among diazotroph taxa. Our ecophysiological model predicted bottom-up effects of mesoscale eddies to vary among diazotrophs, driven by the different adaptations of taxa to light, temperature, and nutrient concentrations. Likewise, eddy-specific grazing varied among diazotroph taxa, with some taxa being grazed upon more in cyclones and others being grazed upon more in anticyclones. Physical accumulation via frontal downwelling appeared to drive the elevated abundance of *Trichodesmium* and *Richelia* at the cyclonic side of the eddy-eddy front in 2017, but apparently did not affect the abundances of smaller, less buoyant taxa. Unfortunately, we were not able to assess eddy-driven mechanisms for some potentially important diazotroph taxa, including UCYN-A, whose growth and grazing could not be predicted due to the lack of culture data and the size constraints of IFCb imaging. Nevertheless, our results suggest that eddy effects on small diazotrophs like *Crocosphaera* are mostly due to biological effects (the net effects of growth and grazing), while eddy effects on large diazotrophs (*Trichodesmium* and DDAs) may be more affected by physical mechanisms.

Finally, changes in the properties of eddies through age and stage further complicate generalizing eddy effects. Mesoscale eddies are evolving features that intensify (with increasingly positive or negative SLA), reach a stable phase, and finally decay over the timescales of months (Sweeney et al., 2003). Though cyclonic and anticyclonic eddies are commonly associated with isopycnal uplift/depression and nutrient injection/dilution in the lower euphotic zone, respectively, in reality, vertical motions and nutrient fluxes vary with eddy age and stage (Barone et al., 2022; McGillicuddy & Robinson, 1997). Our eddy observations, sampled over the timescales of days, represent snapshots of evolving features; we expect the eddy-induced mechanisms discussed above to vary through the lifetime of an eddy. At the time of sampling, both anticyclones were in a stable phase and both cyclones were in a weakening phase (Table S1 in Supporting Information S1), so these four observations are insufficient to deduce the effects of eddy stage on NFRs.

5. Conclusions

Here, we report anomalously high NFRs in two anticyclonic eddies in the NPSG. We coupled diverse datasets and ecological models to explore the mechanisms driving this pattern. Our analyses suggest that the 2017 anticyclone modulated bottom-up (via a reduction in PO_4^{3-} limitation) and top-down (via eddy-specific grazing) control, allowing for the net accumulation of *Crocosphaera* cells, and ultimately, high NFRs. This mechanism may drive high NFRs in other anticyclonic eddies in the NPSG, where surface PO_4^{3-} concentrations are significantly higher in anticyclones than in cyclones (Barone et al., 2019), especially during the summer months of peak *Crocosphaera* abundance. However, no drivers we tested appear to explain the results of our 2018 expedition, for which the high NFR observed in the anticyclonic eddy remains enigmatic. The biological and physical mechanisms through which eddies influence NFRs vary with season, diazotroph community composition, and eddy age or stage. Future efforts may benefit from assessing the ecological controls of uncultivated diazotrophs and from temporal measurements throughout the lifetime of eddies to better understand how eddies might affect successional patterns of diazotrophic communities and measured bulk NFRs.

Data Availability Statement

NFRs and diazotroph abundances, measured by ddPCR and automated flow cytometry, along with environmental data and model output from the eddy cruises can be accessed at https://doi.org/10.5281/zenodo.7540299. IFCb images and time-series are available at http://ifcb-data.soest.hawaii.edu/MESOSCOPE (2017) and http://ifcb-data.soest.hawaii.edu/SCOPEIFCB (2018). Metatranscriptome sequences are available on the NCBI SRA under project numbers PRJNA596510 and PRJNA515070. NFRs and diazotroph *nifH* gene abundances from the HOT program can be accessed under https://doi.org/10.5281/zenodo.3718435, https://doi.org/10.5281/zenodo.6341629, and https://doi.org/10.5281/zenodo.4477269.

Acknowledgments
This work was funded by the Simons Foundation (Award # 721252 to DMK, 721256 to AEW, 721223 to EFD, 721221 to MJC, 721244 to EVA, 721225 to STD, 329108 to SJ, and 724220 to JPZ) and expedition funding from the Schmidt Ocean Institute for R/V *Falkor* Cruise FK180310 in 2018. We are thankful to the chief scientists, including Benedetto Barone (who also provided valuable contributions to drafting and revising the manuscript), Tara Clemente (2017), and Steve Poulos (2018), as well as the captains and crew members of the eddy cruises. We are also grateful to Eric Shimabukuro, Ryan Tabata, and Tim Burrell for their help with field operations, as well as Katie Watkins-Brandt for valuable support with the IFCb on the 2017 expedition.

References

Aldeco-Ramírez, J., Monreal-Gómez, M., Signoret, M., Salas-de-León, D., & Hernández-Becerril, D. (2009). Occurrence of a subsurface anticyclonic eddy, fronts, and *Trichodesmium* spp. *Ciencias Marinas*, *35*(4), 333–344. https://doi.org/10.7773/cm.v35i4.1551

Azimuddin, K. M., Hirai, J., Suzuki, S., Haider, M. N., Tachibana, A., Watanabe, K., et al. (2016). Possible association of diazotrophs with marine zooplankton in the Pacific Ocean. *Microbiologica*, *5*(6), 1016–1026. https://doi.org/10.1002/mbo3.385

Bach, L. T., Riebesell, U., Sett, S., Febiri, S., Rzepka, P., & Schulz, K. G. (2012). An approach for particle sinking velocity measurements in the 3–400 μm size range and considerations on the effect of temperature on sinking rates. *Marine Biology*, *159*(8), 1853–1864. https://doi.org/10.1007/s00227-012-1945-2

Barone, B., Church, M. J., Dugenne, M., Hawco, N. J., Jahn, O., White, A. E., et al. (2022). Biogeochemical dynamics in adjacent mesoscale eddies of opposite polarity. *Global Biogeochemical Cycles*, *36*(2), e2021GB007115. https://doi.org/10.1029/2021gb007115

Barone, B., Coenen, A. R., Beckett, S. J., McGillicuddy, D. J., Weitz, J. S., & Karl, D. M. (2019). The ecological and biogeochemical state of the North Pacific Subtropical Gyre is linked to sea surface height. *Journal of Marine Research*, *77*(2), 215–245. https://doi.org/10.1357/002224019828474241

Benavides, M., Agawin, N. S., Arístegui, J., Ferriol, P., & Stal, L. J. (2011). Nitrogen fixation by *Trichodesmium* and small diazotrophs in the subtropical northeast Atlantic. *Aquatic Microbial Ecology*, *65*(1), 43–53. https://doi.org/10.3354/ame01534

Benitez-Nelson, C. R., Bidigare, R. R., Dickey, T. D., Landry, M. R., Leonard, C. L., Brown, S. L., et al. (2007). Mesoscale eddies drive increased silica export in the subtropical Pacific Ocean. *Science*, *316*(5827), 1017–1021. https://doi.org/10.1126/science.1136221

Berman-Frank, I., Bidle, K. D., Haramaty, L., & Falkowski, P. G. (2004). The demise of the marine cyanobacterium, *Trichodesmium* spp., via an autocatalyzed cell death pathway. *Limnology & Oceanography*, *49*(4), 997–1005. https://doi.org/10.4319/lo.2004.49.4.0997

Boatman, T. G., Davey, P. A., Lawson, T., & Geider, R. J. (2018). The physiological cost of diazotrophy for *Trichodesmium erythraeum* IMS101. *PLoS One*, *13*(4), e0195638. https://doi.org/10.1371/journal.pone.0195638

Boström, K. H., Simu, K., Hagström, Å., & Riemann, L. (2004). Optimization of DNA extraction for quantitative marine bacterioplankton community analysis. *Limnology and Oceanography: Methods*, *2*(11), 365–373. https://doi.org/10.4319/lom.2004.2.365

Böttjer, D., Dore, J. E., Karl, D. M., Letelier, R. M., Mahaffey, C., Wilson, S. T., et al. (2017). Temporal variability of nitrogen fixation and particulate nitrogen export at Station ALOHA. *Limnology & Oceanography*, *62*(1), 200–216. https://doi.org/10.1002/lno.10386

Böttjer, D., Karl, D. M., Letelier, R. M., Viviani, D. A., & Church, M. J. (2014). Experimental assessment of diazotroph responses to elevated seawater pCO_2 in the North Pacific Subtropical Gyre. *Global Biogeochemical Cycles*, *28*(6), 601–616. https://doi.org/10.1002/2013gb004690

Cheung, S., Nitanai, R., Tsurumoto, C., Endo, H., Nakaoka, S. I., Cheah, W., et al. (2020). Physical forcing controls the basin-scale occurrence of nitrogen-fixing organisms in the North Pacific Ocean. *Global Biogeochemical Cycles*, *34*(9), e2019GB006452. https://doi.org/10.1029/2019gb006452

Church, M. J., Björkman, K. M., Karl, D. M., Saito, M. A., & Zehr, J. P. (2008). Regional distributions of nitrogen-fixing bacteria in the Pacific Ocean. *Limnology & Oceanography*, *53*(1), 63–77. https://doi.org/10.4319/lo.2008.53.1.0063

Church, M. J., Jenkins, B. D., Karl, D. M., & Zehr, J. P. (2005). Vertical distributions of nitrogen-fixing phylotypes at Stn ALOHA in the oligotrophic North Pacific Ocean. *Aquatic Microbial Ecology*, *38*(1), 3–14. https://doi.org/10.3354/ame038003

Church, M. J., Mahaffey, C., Letelier, R. M., Lukas, R., Zehr, J. P., & Karl, D. M. (2009). Physical forcing of nitrogen fixation and diazotroph community structure in the North Pacific subtropical gyre. *Global Biogeochemical Cycles*, *23*(2), GB2020. https://doi.org/10.1029/2008gb003418

Church, M. J., Short, C. M., Jenkins, B. D., Karl, D. M., & Zehr, J. P. (2005). Temporal patterns of nitrogenase gene (*nifH*) expression in the oligotrophic North Pacific Ocean. *Applied and Environmental Microbiology*, *71*(9), 5362–5370. https://doi.org/10.1128/aem.71.9.5362-5370.2005

Conroy, B. J., Steinberg, D. K., Song, B., Kalmbach, A., Carpenter, E. J., & Foster, R. A. (2017). Mesozooplankton graze on cyanobacteria in the Amazon river plume and western tropical North Atlantic. *Frontiers in Microbiology*, *8*, 1436. https://doi.org/10.3389/fmicb.2017.01436

Crawley, M. J. (2013). *The R book*. John Wiley & Sons Ltd.

D'Asaro, E. A., Shcherbina, A. Y., Klymak, J. M., Molemaker, J., Novelli, G., Guigand, C. M., et al. (2018). Ocean convergence and the dispersion of flotsam. *Proceedings of the National Academy of Sciences of the United States of America*, *115*(6), 1162–1167. https://doi.org/10.1073/pnas.1718453115

Davis, C. S., & McGillicuddy, D. J. (2006). Transatlantic abundance of the N_2-fixing colonial cyanobacterium *Trichodesmium*. *Science*, *312*(5779), 1517–1520. https://doi.org/10.1126/science.1123570

de Boyer Montégut, C., Madec, G., Fischer, A. S., Lazar, A., & Iudicone, D. (2004). Mixed layer depth over the global ocean: An examination of profile data and a profile-based climatology. *Journal of Geophysical Research*, *109*(C12), C12003. https://doi.org/10.1029/2004jc002378

Dugenne, M., Henderikx Freitas, F., Wilson, S. T., Karl, D. M., & White, A. E. (2020). Life and death of *Crocosphaera* sp. in the Pacific Ocean: Fine scale predator–prey dynamics. *Limnology & Oceanography*, *65*(11), 2603–2617. https://doi.org/10.1002/lno.11473

Dyhrman, S., Chappell, P., Haley, S., Moffett, J., Orchard, E., Waterbury, J., & Webb, E. (2006). Phosphonate utilization by the globally important marine diazotroph *Trichodesmium*. *Nature*, *439*(7072), 68–71. https://doi.org/10.1038/nature04203

Dyhrman, S. T., & Haley, S. T. (2006). Phosphorus scavenging in the unicellular marine diazotroph *Crocosphaera watsonii*. *Applied and Environmental Microbiology*, *72*(2), 1452–1458. https://doi.org/10.1128/aem.72.2.1452-1458.2006

Farnelid, H., Andersson, A. F., Bertilsson, S., Al-Soud, W. A., Hansen, L. H., Sørensen, S., et al. (2011). Nitrogenase gene amplicons from global marine surface waters are dominated by genes of non-cyanobacteria. *PLoS One*, *6*(4), e19223. https://doi.org/10.1371/journal.pone.0019223

Ferrón, S., del Valle, D. A., Björkman, K. M., Quay, P. D., Church, M. J., & Karl, D. M. (2016). Application of membrane inlet mass spectrometry to measure aquatic gross primary production by the ^{18}O *in vitro* method. *Limnology and Oceanography: Methods*, *14*(9), 610–622. https://doi.org/10.1002/lom3.10116

Fitzsimmons, J. N., Hayes, C. T., Al-Subiai, S. N., Zhang, R., Morton, P. L., Weisend, R. E., et al. (2015). Daily to decadal variability of size-fractionated iron and iron-binding ligands at the Hawaii Ocean Time-series Station ALOHA. *Geochimica et Cosmochimica Acta*, *171*, 303–324. https://doi.org/10.1016/j.gca.2015.08.012

Follett, C. L., Dutkiewicz, S., Karl, D. M., Inomura, K., & Follows, M. J. (2018). Seasonal resource conditions favor a summertime increase in North Pacific diatom–diazotroph associations. *The ISME Journal*, *12*(6), 1543–1557. https://doi.org/10.1038/s41396-017-0012-x

Fong, A. A., Karl, D. M., Lukas, R., Letelier, R. M., Zehr, J. P., & Church, M. J. (2008). Nitrogen fixation in an anticyclonic eddy in the oligotrophic North Pacific Ocean. *The ISME Journal*, *2*(6), 663–676. https://doi.org/10.1038/ismej.2008.22

Foreman, R. K., Segura-Noguera, M., & Karl, D. M. (2016). Validation of Ti (III) as a reducing agent in the chemiluminescent determination of nitrate and nitrite in seawater. *Marine Chemistry*, *186*, 83–89. https://doi.org/10.1016/j.marchem.2016.08.003

Foster, R., Subramaniam, A., Mahaffey, C., Carpenter, E., Capone, D., & Zehr, J. (2007). Influence of the Amazon River plume on distributions of free-living and symbiotic cyanobacteria in the western tropical North Atlantic Ocean. *Limnology & Oceanography*, *52*(2), 517–532. https://doi.org/10.4319/lo.2007.52.2.0517

Gaube, P., Chelton, D. B., Samelson, R. M., Schlax, M. G., & O'Neill, L. W. (2015). Satellite observations of mesoscale eddy-induced Ekman pumping. *Journal of Physical Oceanography*, *45*(1), 104–132. https://doi.org/10.1175/jpo-d-14-0032.1

Gifford, S. M., Becker, J. W., Sosa, O. A., Repeta, D. J., & DeLong, E. F. (2016). Quantitative transcriptomics reveals the growth-and nutrient-dependent response of a streamlined marine methylotroph to methanol and naturally occurring dissolved organic matter. *mBio*, *7*(6), e01279–e01216. https://doi.org/10.1128/mbio.01279-16

Gradoville, M. R., Cabello, A. M., Wilson, S. T., Turk-Kubo, K. A., Karl, D. M., & Zehr, J. P. (2021). Light and depth dependency of nitrogen fixation by the non-photosynthetic, symbiotic cyanobacterium UCYN-A. *Environmental Microbiology*, *23*(8), 4518–4531. https://doi.org/10.1111/1462-2920.15645

Gradoville, M. R., Dugenne, M., Hynes, A. M., Zehr, J. P., & White, A. E. (2022). Empirical relationship between *nif*H gene abundance and diazotroph cell concentration in the North Pacific Subtropical Gyre. *Journal of Phycology*, *58*(6), 829–833. Portico. https://doi.org/10.1111/jpy.13289

Gradoville, M. R., Farnelid, H., White, A. E., Turk-Kubo, K. A., Stewart, B., Ribalet, F., et al. (2020). Latitudinal constraints on the abundance and activity of the cyanobacterium UCYN-A and other marine diazotrophs in the North Pacific. *Limnology & Oceanography*, *65*(8), 1858–1875. https://doi.org/10.1002/lno.11423

Guidi, L., Calil, P. H., Duhamel, S., Björkman, K. M., Doney, S. C., Jackson, G. A., et al. (2012). Does eddy-eddy interaction control surface phytoplankton distribution and carbon export in the North Pacific Subtropical Gyre? *Journal of Geophysical Research*, *117*(G2), G02024. https://doi.org/10.1029/2012jg001984

Harke, M. J., Frischkorn, K. R., Hennon, G. M., Haley, S. T., Barone, B., Karl, D. M., & Dyhrman, S. T. (2021). Microbial community transcriptional patterns vary in response to mesoscale forcing in the North Pacific Subtropical Gyre. *Environmental Microbiology*, *23*(8), 4807–4822. https://doi.org/10.1111/1462-2920.15677

Hawco, N. J., Barone, B., Church, M. J., Babcock-Adams, L., Repeta, D. J., Wear, E. K., et al. (2021). Iron depletion in the deep chlorophyll maximum: Mesoscale eddies as natural iron fertilization experiments. *Global Biogeochemical Cycles*, *35*(12), e2021GB007112. https://doi.org/10.1029/2021gb007112

Hewson, I., Govil, S. R., Capone, D. G., Carpenter, E. J., & Fuhrman, J. A. (2004). Evidence of *Trichodesmium* viral lysis and potential significance for biogeochemical cycling in the oligotrophic ocean. *Aquatic Microbial Ecology*, *36*(1), 1–8. https://doi.org/10.3354/ame036001

Holl, C. M., Waite, A. M., Pesant, S., Thompson, P. A., & Montoya, J. P. (2007). Unicellular diazotrophy as a source of nitrogen to Leeuwin Current coastal eddies. *Deep Sea Research Part II: Topical Studies in Oceanography*, *54*(8–10), 1045–1054. https://doi.org/10.1016/j.dsr2.2007.02.002

Hoppe, K. S. (2013). *The sinking rate and transparent exopolymer particle (TEP) production of Hemiaulus hauckii*. Doctoral dissertation. University of Texas at Austin.

Hunt, B. P., Bonnet, S., Berthelot, H., Conroy, B. J., Foster, R. A., & Pagano, M. (2016). Contribution and pathways of diazotroph-derived nitrogen to zooplankton during the VAHINE mesocosm experiment in the oligotrophic New Caledonia lagoon. *Biogeosciences*, *13*(10), 3131–3145. https://doi.org/10.5194/bg-13-3131-2016

Jassby, A. D., & Platt, T. (1976). Mathematical formulation of the relationship between photosynthesis and light for phytoplankton. *Limnology & Oceanography*, *21*(4), 540–547. https://doi.org/10.4319/lo.1976.21.4.0540

Jeong, H. J., Yoo, Y. D., Kim, J. S., Seong, K. A., Kang, N. S., & Kim, T. H. (2010). Growth, feeding and ecological roles of the mixotrophic and heterotrophic dinoflagellates in marine planktonic food webs. *Ocean Science Journal*, *45*(2), 65–91. https://doi.org/10.1007/s12601-010-0007-2

Karl, D., Christian, J., Dore, J., Hebel, D., Letelier, R., Tupas, L., & Winn, C. (1996). Seasonal and interannual variability in primary production and particle flux at Station ALOHA. *Deep Sea Research Part II: Topical Studies in Oceanography*, *43*(2–3), 539–568. https://doi.org/10.1016/0967-0645(96)00002-1

Karl, D., Letelier, R., Tupas, L., Dore, J., Christian, J., & Hebel, D. (1997). The role of nitrogen fixation in biogeochemical cycling in the subtropical North Pacific Ocean. *Nature*, *388*(6642), 533–538. https://doi.org/10.1038/41474

Karl, D., Michaels, A., Bergman, B., Capone, D., Carpenter, E., Letelier, R., et al. (2002). Dinitrogen fixation in the world's oceans. *Biogeochemistry*, *57*(1), 47–98. https://doi.org/10.1023/a:1015798105851

Karl, D. M., & Church, M. J. (2014). Microbial oceanography and the Hawaii Ocean Time-series programme. *Nature Reviews Microbiology*, *12*(10), 699–713. https://doi.org/10.1038/nrmicro3333

Karl, D. M., Church, M. J., Dore, J. E., Letelier, R. M., & Mahaffey, C. (2012). Predictable and efficient carbon sequestration in the North Pacific Ocean supported by symbiotic nitrogen fixation. *Proceedings of the National Academy of Sciences of the United States of America*, *109*(6), 1842–1849. https://doi.org/10.1073/pnas.1120312109

Karl, D. M., & Tien, G. (1992). MAGIC: A sensitive and precise method for measuring dissolved phosphorus in aquatic environments. *Limnology & Oceanography*, *37*(1), 105–116. https://doi.org/10.4319/lo.1992.37.1.0105

Landolfi, A., Prowe, A., Pahlow, M., Somes, C. J., Chien, C.-T., Schartau, M., et al. (2021). Can top-down controls expand the ecological niche of marine N_2 fixers? *Frontiers in Microbiology*, *12*, 690200. https://doi.org/10.3389/fmicb.2021.690200

Landry, M. R., Brown, S. L., Rii, Y. M., Selph, K. E., Bidigare, R. R., Yang, E. J., & Simmons, M. P. (2008). Depth-stratified phytoplankton dynamics in Cyclone Opal, a subtropical mesoscale eddy. *Deep Sea Research Part II: Topical Studies in Oceanography*, *55*(10–13), 1348–1359. https://doi.org/10.1016/j.dsr2.2008.02.001

Letelier, R. M., Björkman, K. M., Church, M. J., Hamilton, D. S., Mahowald, N. M., Scanza, R. A., et al. (2019). Climate-driven oscillation of phosphorus and iron limitation in the North Pacific Subtropical Gyre. *Proceedings of the National Academy of Sciences of the United States of America*, *116*(26), 12720–12728. https://doi.org/10.1073/pnas.1900789116

Letelier, R. M., White, A. E., Bidigare, R. R., Barone, B., Church, M. J., & Karl, D. M. (2017). Light absorption by phytoplankton in the North Pacific subtropical Gyre. *Limnology & Oceanography*, *62*(4), 1526–1540. https://doi.org/10.1002/lno.10515

Liu, J., Zhou, L., Li, J., Lin, Y., Ke, Z., Zhao, C., et al. (2020). Effect of mesoscale eddies on diazotroph community structure and nitrogen fixation rates in the South China Sea. *Regional Studies in Marine Science*, *35*, 101106. https://doi.org/10.1016/j.rsma.2020.101106

Löscher, C., Bourbonnais, A., Dekaezemacker, J., Charoenpong, C. N., Altabet, M. A., Bange, H. W., et al. (2016). N_2 fixation in eddies of the eastern tropical South Pacific Ocean. *Biogeosciences*, *13*(10), 2889–2899. https://doi.org/10.5194/bg-13-2889-2016

Luo, E., Eppley, J. M., Romano, A. E., Mende, D. R., & DeLong, E. F. (2020). Double-stranded DNA virioplankton dynamics and reproductive strategies in the oligotrophic open ocean water column. *The ISME Journal*, *14*(5), 1304–1315. https://doi.org/10.1038/s41396-020-0604-8

Luo, Y.-W., Lima, I., Karl, D., Deutsch, C., & Doney, S. (2014). Data-based assessment of environmental controls on global marine nitrogen fixation. *Biogeosciences*, *11*(3), 691–708. https://doi.org/10.5194/bg-11-691-2014

Mahadevan, A. (2016). The impact of submesoscale physics on primary productivity of plankton. *Annual Review of Marine Science*, *8*(1), 161–184. https://doi.org/10.1146/annurev-marine-010814-015912

McGillicuddy, D., Jr. (2016). Mechanisms of physical-biological-biogeochemical interaction at the oceanic mesoscale. *Annual Review of Marine Science*, *8*(1), 125–159. https://doi.org/10.1146/annurev-marine-010814-015606

McGillicuddy, D., Jr., & Robinson, A. (1997). Eddy-induced nutrient supply and new production in the Sargasso Sea. *Deep Sea Research Part I: Oceanographic Research Papers*, *44*(8), 1427–1450. https://doi.org/10.1016/s0967-0637(97)00024-1

McGillicuddy, D. J., Jr. (2014). Do *Trichodesmium* spp. populations in the North Atlantic export most of the nitrogen they fix? *Global Biogeochemical Cycles*, *28*(2), 103–114. https://doi.org/10.1002/2013gb004652

Mohr, W., Großkopf, T., Wallace, D. W. R., & LaRoche, J. (2010). Methodological underestimation of oceanic nitrogen fixation rates. *PLoS One*, *5*(9), e12583. https://doi.org/10.1371/journal.pone.0012583

Moisander, P. H., Beinart, R. A., Hewson, I., White, A. E., Johnson, K. S., Carlson, C. A., et al. (2010). Unicellular cyanobacterial distributions broaden the oceanic N_2 fixation domain. *Science*, *327*(5972), 1512–1514. https://doi.org/10.1126/science.1185468

Moisander, P. H., Beinart, R. A., Voss, M., & Zehr, J. P. (2008). Diversity and abundance of diazotrophic microorganisms in the South China Sea during intermonsoon. *The ISME Journal*, *2*(9), 954–967. https://doi.org/10.1038/ismej.2008.51

Moisander, P. H., Benavides, M., Bonnet, S., Berman-Frank, I., White, A. E., & Riemann, L. (2017). Chasing after non-cyanobacterial nitrogen fixation in marine pelagic environments. *Frontiers in Microbiology*, *8*, 1736. https://doi.org/10.3389/fmicb.2017.01736

Montoya, J. P., Voss, M., Kahler, P., & Capone, D. G. (1996). A simple, high-precision, high-sensitivity tracer assay for N_2 fixation. *Applied and Environmental Microbiology*, *62*(3), 986–993. https://doi.org/10.1128/aem.62.3.986-993.1996

Mulholland, M. (2007). The fate of nitrogen fixed by diazotrophs in the ocean. *Biogeosciences*, *4*(1), 37–51. https://doi.org/10.5194/bg-4-37-2007

Olson, E. M., McGillicuddy, D. J., Flierl, G. R., Davis, C. S., Dyhrman, S. T., & Waterbury, J. B. (2015). Mesoscale eddies and *Trichodesmium* spp. distributions in the southwestern North Atlantic. *Journal of Geophysical Research: Oceans*, *120*(6), 4129–4150. https://doi.org/10.1002/2015jc010728

O'Neil, J., Metzler, P., & Glibert, P. (1996). Ingestion of $^{15}N_2$-labelled *Trichodesmium* spp. and ammonium regeneration by the harpacticoid copepod *Macrosetella gracilis*. *Marine Biology*, *125*(1), 89–96. https://doi.org/10.1007/bf00350763

O'Neil, J. M. (1998). The colonial cyanobacterium *Trichodesmium* as a physical and nutritional substrate for the harpacticoid copepod *Macrosetella gracilis*. *Journal of Plankton Research*, *20*(1), 43–59. https://doi.org/10.1093/plankt/20.1.43

O'Neil, J. M., & Roman, M. R. (1992). Grazers and associated organisms of Trichodesmium. In *Marine pelagic cyanobacteria: Trichodesmium and other diazotrophs* (pp. 61–73). Kluwer.

Orchard, E. D., Ammerman, J. W., Lomas, M. W., & Dyhrman, S. T. (2010). Dissolved inorganic and organic phosphorus uptake in *Trichodesmium* and the microbial community: The importance of phosphorus ester in the Sargasso Sea. *Limnology & Oceanography*, *55*(3), 1390–1399. https://doi.org/10.4319/lo.2010.55.3.1390

Parks, D. H., Chuvochina, M., Waite, D. W., Rinke, C., Skarshewski, A., Chaumeil, P.-A., & Hugenholtz, P. (2018). A standardized bacterial taxonomy based on genome phylogeny substantially revises the tree of life. *Nature Biotechnology*, *36*(10), 996–1004. https://doi.org/10.1038/nbt.4229

Pasulka, A. L., Landry, M. R., Taniguchi, D. A., Taylor, A. G., & Church, M. J. (2013). Temporal dynamics of phytoplankton and heterotrophic protists at station ALOHA. *Deep Sea Research Part II: Topical Studies in Oceanography*, *93*, 44–57. https://doi.org/10.1016/j.dsr2.2013.01.007

Pereira, N., Shilova, I. N., & Zehr, J. P. (2016). Molecular markers define progressing stages of phosphorus limitation in the nitrogen-fixing cyanobacterium, *Crocosphaera*. *Journal of Phycology*, *52*(2), 274–282. https://doi.org/10.1111/jpy.12396

Pinedo-González, P., Hawco, N. J., Bundy, R. M., Armbrust, E. V., Follows, M. J., Cael, B., et al. (2020). Anthropogenic Asian aerosols provide Fe to the North Pacific ocean. *Proceedings of the National Academy of Sciences of the United States of America*, *117*(45), 27862–27868. https://doi.org/10.1073/pnas.2010315117

Poff, K. E., Leu, A. O., Eppley, J. M., Karl, D. M., & DeLong, E. F. (2021). Microbial dynamics of elevated carbon flux in the open ocean's abyss. *Proceedings of the National Academy of Sciences United States America*, *118*(4), e2018269118. https://doi.org/10.1073/pnas.2018269118

Rahav, E., Herut, B., Stambler, N., Bar-Zeev, E., Mulholland, M. R., & Berman-Frank, I. (2013). Uncoupling between dinitrogen fixation and primary productivity in the eastern Mediterranean Sea. *Journal of Geophysical Research: Biogeosciences*, *118*(1), 195–202. https://doi.org/10.1002/jgrg.20023

Ribalet, F., Berthiaume, C., Hynes, A., Swalwell, J., Carlson, M., Clayton, S., et al. (2019). SeaFlow data v1, high-resolution abundance, size and biomass of small phytoplankton in the North Pacific. *Scientific Data*, *6*(1), 1–8. https://doi.org/10.1038/s41597-019-0292-2

Rii, Y. M., Peoples, L. M., Karl, D. M., & Church, M. J. (2021). Seasonality and episodic variation in picoeukaryote diversity and structure reveal community resilience to disturbances in the North Pacific Subtropical Gyre. *Limnology & Oceanography*, *67*(S1), S331–S351. https://doi.org/10.1002/lno.11916

Robidart, J. C., Church, M. J., Ryan, J. P., Ascani, F., Wilson, S. T., Bombar, D., et al. (2014). Ecogenomic sensor reveals controls on N_2-fixing microorganisms in the North Pacific Ocean. *The ISME Journal*, *8*(6), 1175–1185. https://doi.org/10.1038/ismej.2013.244

Sargent, E. C., Hitchcock, A., Johansson, S. A., Langlois, R., Moore, C. M., LaRoche, J., et al. (2016). Evidence for polyploidy in the globally important diazotroph *Trichodesmium*. *FEMS Microbiology Letters*, *363*(21), fnw244. https://doi.org/10.1093/femsle/fnw244

Scavotto, R. E., Dziallas, C., Bentzon-Tilia, M., Riemann, L., & Moisander, P. H. (2015). Nitrogen-fixing bacteria associated with copepods in coastal waters of the North Atlantic Ocean. *Environmental Microbiology*, *17*(10), 3754–3765. https://doi.org/10.1111/1462-2920.12777

Schartau, M., Wallhead, P., Hemmings, J., Loptien, U., Kriest, I., Krishna, S., et al. (2017). Reviews and syntheses: Parameter identification in marine planktonic ecosystem modelling. *Biogeosciences*, *14*(6), 1647–1701. https://doi.org/10.5194/bg-14-1647-2017

Snow, J. T., Polyviou, D., Skipp, P., Chrismas, N. A., Hitchcock, A., Geider, R., et al. (2015). Quantifying integrated proteomic responses to iron stress in the globally important marine diazotroph *Trichodesmium*. *PLoS One*, *10*(11), e0142626. https://doi.org/10.1371/journal.pone.0142626

Sosik, H. M., & Olson, R. J. (2007). Automated taxonomic classification of phytoplankton sampled with imaging-in-flow cytometry. *Limnology and Oceanography: Methods*, *5*(6), 204–216. https://doi.org/10.4319/lom.2007.5.204

Stenegren, M. (2020). Significance of N_2 fixing planktonic symbioses for open ocean ecosystems [Doctoral dissertation]. Stockholm University.

Stukel, M. R., Coles, V. J., Brooks, M., & Hood, R. R. (2014). Top-down, bottom-up and physical controls on diatom-diazotroph assemblage growth in the Amazon River plume. *Biogeosciences*, *11*(12), 3259–3278. https://doi.org/10.5194/bg-11-3259-2014

Sweeney, E. N., McGillicuddy, D. J. Jr., & Buesseler, K. O. (2003). Biogeochemical impacts due to mesoscale eddy activity in the Sargasso Sea as measured at the Bermuda Atlantic Time-series Study (BATS). *Deep Sea Research Part II: Topical Studies in Oceanography*, *50*(22–26), 3017–3039. https://doi.org/10.1016/j.dsr2.2003.07.008

Taboada, F. G., Gil, R. G., Höfer, J., González, S., & Anadón, R. (2010). *Trichodesmium* spp. population structure in the eastern North Atlantic subtropical gyre. *Deep Sea Research Part I: Oceanographic Research Papers*, *57*(1), 65–77. https://doi.org/10.1016/j.dsr.2009.09.005

Tang, W., Li, Z., & Cassar, N. (2019). Machine learning estimates of global marine nitrogen fixation. *Journal of Geophysical Research: Biogeosciences*, *124*(3), 717–730. https://doi.org/10.1029/2018jg004828

Tibshirani, R., Bien, J., Friedman, J., Hastie, T., Simon, N., Taylor, J., & Tibshirani, R. J. (2012). Strong rules for discarding predictors in lasso-type problems. *Journal of the Royal Statistical Society: Series B*, *74*(2), 245–266. https://doi.org/10.1111/j.1467-9868.2011.01004.x

Tuo, S. (2015). The distributions and the mechanisms of the cyanobionts and their host diatoms in the northern South China Sea and the Kuroshio [Doctoral dissertation]. National Sun Yat-sen University.

Villareal, T., & Carpenter, E. (2003). Buoyancy regulation and the potential for vertical migration in the oceanic cyanobacterium *Trichodesmium*. *Microbial Ecology*, *45*(1), 1–10. https://doi.org/10.1007/s00248-002-1012-5

Villareal, T. A., & Carpenter, E. J. (1989). Nitrogen fixation, suspension characteristics, and chemical composition of *Rhizosolenia* mats in the central North Pacific gyre. *Biological Oceanography*, *6*(3–4), 327–345.

Walsby, A. (1978). The properties and buoyancy-providing role of gas vacuoles in *Trichodesmium* Ehrenberg. *British Phycological Journal*, *13*(2), 103–116. https://doi.org/10.1080/00071617800650121

Ward, B. A., Dutkiewicz, S., Moore, C. M., & Follows, M. J. (2013). Iron, phosphorus, and nitrogen supply ratios define the biogeography of nitrogen fixation. *Limnology & Oceanography*, *58*(6), 2059–2075. https://doi.org/10.4319/lo.2013.58.6.2059

Webb, E. A., Ehrenreich, I. M., Brown, S. L., Valois, F. W., & Waterbury, J. B. (2009). Phenotypic and genotypic characterization of multiple strains of the diazotrophic cyanobacterium, *Crocosphaera watsonii*, isolated from the open ocean. *Environmental Microbiology*, *11*(2), 338–348. https://doi.org/10.1111/j.1462-2920.2008.01771.x

White, A. E., Granger, J., Selden, C., Gradoville, M. R., Potts, L., Bourbonnais, A., et al. (2020). A critical review of the $^{15}N_2$ tracer method to measure diazotrophic production in pelagic ecosystems. *Limnology and Oceanography: Methods*, *18*(4), 129–147. https://doi.org/10.1002/lom3.10353

White, A. E., Karl, D. M., Björkman, K. M., Beversdorf, L. J., & Letelier, R. M. (2010). Production of organic matter by *Trichodesmium* IMS101 as a function of phosphorus source. *Limnology & Oceanography*, *55*(4), 1755–1767. <Go to ISI>://WOS:000283657000023. https://doi.org/10.4319/lo.2010.55.4.1755

Wilson, S. T., Aylward, F. O., Ribalet, F., Barone, B., Casey, J. R., Connell, P. E., et al. (2017). Coordinated regulation of growth, activity and transcription in natural populations of the unicellular nitrogen-fixing cyanobacterium *Crocosphaera*. *Nature Microbiology*, *2*(9), 17118. https://doi.org/10.1038/nmicrobiol.2017.118

Wilson, S. T., Böttjer, D., Church, M. J., & Karl, D. M. (2012). Comparative assessment of nitrogen fixation methodologies, conducted in the oligotrophic North Pacific Ocean. *Applied and Environmental Microbiology*, *78*(18), 6516–6523. https://doi.org/10.1128/aem.01146-12

Wozniak, B., Dera, J., Ficek, D., Majchrowski, R., Ostrowska, M., & Kaczmarek, S. (2003). Modelling light and photosynthesis in the marine environment. *Oceanologia*, *45*(2), 171–245.

Yoder, J. A., Ackleson, S. G., Barber, R. T., Flament, P., & Balch, W. M. (1994). A line in the sea. *Nature*, *371*(6499), 689–692. https://doi.org/10.1038/371689a0

Zeev, E. B., Yogev, T., Man-Aharonovich, D., Kress, N., Herut, B., Béja, O., & Berman-Frank, I. (2008). Seasonal dynamics of the endosymbiotic, nitrogen-fixing cyanobacterium *Richelia intracellularis* in the eastern Mediterranean Sea. *The ISME Journal*, *2*(9), 911–923. https://doi.org/10.1038/ismej.2008.56

Zehr, J. P., Waterbury, J. B., Turner, P. J., Montoya, J. P., Omoregie, E., Steward, G. F., et al. (2001). Unicellular cyanobacteria fix N_2 in the subtropical North Pacific Ocean. *Nature*, *412*(6847), 635–637. https://doi.org/10.1038/35088063